DESY 97-075
April 1997

ISSN 0418-9833

Bose-Einstein Correlations in Deep Inelastic ep Scattering at HERA

H1 Collaboration

Abstract

Two-particle correlations in invariant mass are studied separately for like-sign and unlike-sign charged particles produced in deep inelastic positron-proton scattering in a new kinematical domain. The data were taken with the H1 detector at the HERA storage ring in 1994, in which 27.5 GeV positrons collided with 820 GeV protons at a centre of mass energy $\sqrt{s} = 300$ GeV.

The observed enhancement of the like-sign correlations at low invariant masses is related to the dimensions of the hadronic source. The data are compared to different QCD models where the hadronization is performed with the string-fragmentation model. Results are presented for the first time separately for diffractive and non-diffractive scattering, in domains of four-momentum transfer, Bjorken-x, and hadronic center of mass energy, and in intervals of charged particle multiplicity. The observed source radii do not differ strongly from those measured in lower energy lepton-nucleon inelastic scattering, and e^+e^- annihilation.

C. Adloff[35], S. Aid[13], M. Anderson[23], V. Andreev[26], B. Andrieu[29], V. Arkadov[36], C. Arndt[11], I. Ayyaz[30], A. Babaev[25], J. Bähr[36], J. Bán[18], Y. Ban[28], P. Baranov[26], E. Barrelet[30], R. Barschke[11], W. Bartel[11], U. Bassler[30], H.P. Beck[38], M. Beck[14], H.-J. Behrend[11], A. Belousov[26], Ch. Berger[1], G. Bernardi[30], G. Bertrand-Coremans[4], R. Beyer[11], P. Biddulph[23], P. Bispham[23], J.C. Bizot[28], K. Borras[8], F. Botterweck[27], V. Boudry[29], S. Bourov[25], A. Braemer[15], W. Braunschweig[1], V. Brisson[28], W. Brückner[14], P. Bruel[29], D. Bruncko[18], C. Brune[16], R. Buchholz[11], L. Büngener[13], J. Bürger[11], F.W. Büsser[13], A. Buniatian[4], S. Burke[19], M.J. Burton[23], G. Buschhorn[27], D. Calvet[24], A.J. Campbell[11], T. Carli[27], M. Charlet[11], D. Clarke[5], B. Clerbaux[4], S. Cocks[20], J.G. Contreras[8], C. Cormack[20], J.A. Coughlan[5], A. Courau[28], M.-C. Cousinou[24], B.E. Cox[23], G. Cozzika[9], D.G. Cussans[5], J. Cvach[31], S. Dagoret[30], J.B. Dainton[20], W.D. Dau[17], K. Daum[40], M. David[9], C.L. Davis[19,41], A. De Roeck[11], E.A. De Wolf[4], B. Delcourt[28], M. Dirkmann[8], P. Dixon[19], W. Dlugosz[7], C. Dollfus[38], K.T. Donovan[21], J.D. Dowell[3], H.B. Dreis[2], A. Droutskoi[25], J. Ebert[35], T.R. Ebert[20], G. Eckerlin[11], V. Efremenko[25], S. Egli[38], R. Eichler[37], F. Eisele[15], E. Eisenhandler[21], E. Elsen[11], M. Erdmann[15], A.B. Fahr[13], L. Favart[28], A. Fedotov[25], R. Felst[11], J. Feltesse[9], J. Ferencei[18], F. Ferrarotto[33], K. Flamm[11], M. Fleischer[8], M. Flieser[27], G. Flügge[2], A. Fomenko[26], J. Formánek[32], J.M. Foster[23], G. Franke[11], E. Gabathuler[20], K. Gabathuler[34], F. Gaede[27], J. Garvey[3], J. Gayler[11], M. Gebauer[36], H. Genzel[1], R. Gerhards[11], A. Glazov[36], L. Goerlich[6], N. Gogitidze[26], M. Goldberg[30], D. Goldner[8], K. Golec-Biernat[6], B. Gonzalez-Pineiro[30], I. Gorelov[25], C. Grab[37], H. Grässler[2], T. Greenshaw[20], R.K. Griffiths[21], G. Grindhammer[27], A. Gruber[27], C. Gruber[17], T. Hadig[1], D. Haidt[11], L. Hajduk[6], T. Haller[14], M. Hampel[1], W.J. Haynes[5], B. Heinemann[11], G. Heinzelmann[13], R.C.W. Henderson[19], H. Henschel[36], I. Herynek[31], M.F. Hess[27], K. Hewitt[3], K.H. Hiller[36], C.D. Hilton[23], J. Hladký[31], M. Höppner[8], D. Hoffmann[11], T. Holtom[20], R. Horisberger[34], V.L. Hudgson[3], M. Hütte[8], M. Ibbotson[23], Ç. İşsever[8], H. Itterbeck[1], A. Jacholkowska[28], C. Jacobsson[22], M. Jacquet[28], M. Jaffre[28], J. Janoth[16], D.M. Jansen[14], L. Jönsson[22], D.P. Johnson[4], H. Jung[22], P.I.P Kalmus[21], M. Kander[11], D. Kant[21], U. Kathage[17], J. Katzy[15], H.H. Kaufmann[36], O. Kaufmann[15], M. Kausch[11], S. Kazarian[11], I.R. Kenyon[3], S. Kermiche[24], C. Keuker[1], C. Kiesling[27], M. Klein[36], C. Kleinwort[11], G. Knies[11], T. Köhler[1], J.H. Köhne[27], H. Kolanoski[39], S.D. Kolya[23], V. Korbel[11], P. Kostka[36], S.K. Kotelnikov[26], T. Krämerkämper[8], M.W. Krasny[6,30], H. Krehbiel[11], D. Krücker[27], A. Küpper[35], H. Küster[22], M. Kuhlen[27], T. Kurča[36], J. Kurzhöfer[8], B. Laforge[9], M.P.J. Landon[21], W. Lange[36], U. Langenegger[37], A. Lebedev[26], F. Lehner[11], V. Lemaitre[11], S. Levonian[29], M. Lindstroem[22], F. Linsel[11], J. Lipinski[11], B. List[11], G. Lobo[28], J.W. Lomas[23], G.C. Lopez[12], V. Lubimov[25], D. Lüke[8,11], L. Lytkin[14], N. Magnussen[35], H. Mahlke-Krüger[11], E. Malinovski[26], R. Maraček[18], P. Marage[4], J. Marks[15], R. Marshall[23], J. Martens[35], G. Martin[13], R. Martin[20], H.-U. Martyn[1], J. Martyniak[6], T. Mavroidis[21], S.J. Maxfield[20], S.J. McMahon[20], A. Mehta[5], K. Meier[16], P. Merkel[11], F. Metlica[14], A. Meyer[13], A. Meyer[11], H. Meyer[35], J. Meyer[11], P.-O. Meyer[2], A. Migliori[29], S. Mikocki[6], D. Milstead[20], J. Moeck[27], F. Moreau[29], J.V. Morris[5], E. Mroczko[6], D. Müller[38], T. Walter[38], K. Müller[11], P. Murín[18], V. Nagovizin[25], R. Nahnhauer[36], B. Naroska[13], Th. Naumann[36], I. Négri[24], P.R. Newman[3], D. Newton[19], H.K. Nguyen[30], T.C. Nicholls[3], F. Niebergall[13], C. Niebuhr[11], Ch. Niedzballa[1], H. Niggli[37], G. Nowak[6], T. Nunnemann[14], M. Nyberg-Werther[22], H. Oberlack[27], J.E. Olsson[11], D. Ozerov[25], P. Palmen[2], E. Panaro[11], A. Panitch[4], C. Pascaud[28], S. Passaggio[37], G.D. Patel[20], H. Pawletta[2], E. Peppel[36], E. Perez[9], J.P. Phillips[20], A. Pieuchot[24], D. Pitzl[37], R. Pöschl[8], G. Pope[7], B. Povh[14], S. Prell[11], K. Rabbertz[1], G. Rädel[11], J. Riedlberger[37],

P. Reimer[31], H. Rick[8], S. Riess[13], E. Rizvi[21], P. Robmann[38], R. Roosen[4], K. Rosenbauer[1], A. Rostovtsev[30], F. Rouse[7], C. Royon[9], K. Rüter[27], S. Rusakov[26], K. Rybicki[6], D.P.C. Sankey[5], P. Schacht[27], S. Schiek[13], S. Schleif[16], P. Schleper[15], W. von Schlippe[21], D. Schmidt[35], G. Schmidt[13], L. Schoeffel[9], A. Schöning[11], V. Schröder[11], E. Schuhmann[27], B. Schwab[15], F. Sefkow[38], A. Semenov[25], V. Shekelyan[11], I. Sheviakov[26], L.N. Shtarkov[26], G. Siegmon[17], U. Siewert[17], Y. Sirois[29], I.O. Skillicorn[10], T. Sloan[19], P. Smirnov[26], M. Smith[20], V. Solochenko[25], Y. Soloviev[26], A. Specka[29], J. Spiekermann[8], S. Spielman[29], H. Spitzer[13], F. Squinabol[28], P. Steffen[11], R. Steinberg[2], J. Steinhart[13], B. Stella[33], A. Stellberger[16], J. Stier[11], J. Stiewe[16], U. Stößlein[36], K. Stolze[36], U. Straumann[15], W. Struczinski[2], J.P. Sutton[3], S. Tapprogge[16], M. Taševský[32], V. Tchernyshov[25], S. Tchetchelnitski[25], J. Theissen[2], G. Thompson[21], P.D. Thompson[3], N. Tobien[11], R. Todenhagen[14], P. Truöl[38], G. Tsipolitis[37], J. Turnau[6], E. Tzamariudaki[11], P. Uelkes[2], A. Usik[26], S. Valkár[32], A. Valkárová[32], C. Vallée[24], P. Van Esch[4], P. Van Mechelen[4], D. Vandenplas[29], Y. Vazdik[26], P. Verrecchia[9], G. Villet[9], K. Wacker[8], A. Wagener[2], M. Wagener[34], R. Wallny[15], B. Waugh[23], G. Weber[13], M. Weber[16], D. Wegener[8], A. Wegner[27], T. Wengler[15], M. Werner[15], L.R. West[3], S. Wiesand[35], T. Wilksen[11], S. Willard[7], M. Winde[36], G.-G. Winter[11], C. Wittek[13], M. Wobisch[2], H. Wollatz[11], E. Wünsch[11], J. Žáček[32], D. Zarbock[12], Z. Zhang[28], A. Zhokin[25], P. Zini[30], F. Zomer[28], J. Zsembery[9], and M. zur Nedden[38].

[1] *I. Physikalisches Institut der RWTH, Aachen, Germany*[a]
[2] *III. Physikalisches Institut der RWTH, Aachen, Germany*[a]
[3] *School of Physics and Space Research, University of Birmingham, Birmingham, UK*[b]
[4] *Inter-University Institute for High Energies ULB-VUB, Brussels; Universitaire Instelling Antwerpen, Wilrijk; Belgium*[c]
[5] *Rutherford Appleton Laboratory, Chilton, Didcot, UK*[b]
[6] *Institute for Nuclear Physics, Cracow, Poland*[d]
[7] *Physics Department and IIRPA, University of California, Davis, California, USA*[e]
[8] *Institut für Physik, Universität Dortmund, Dortmund, Germany*[a]
[9] *CEA, DSM/DAPNIA, CE-Saclay, Gif-sur-Yvette, France*
[10] *Department of Physics and Astronomy, University of Glasgow, Glasgow, UK*[b]
[11] *DESY, Hamburg, Germany*[a]
[12] *I. Institut für Experimentalphysik, Universität Hamburg, Hamburg, Germany*[a]
[13] *II. Institut für Experimentalphysik, Universität Hamburg, Hamburg, Germany*[a]
[14] *Max-Planck-Institut für Kernphysik, Heidelberg, Germany*[a]
[15] *Physikalisches Institut, Universität Heidelberg, Heidelberg, Germany*[a]
[16] *Institut für Hochenergiephysik, Universität Heidelberg, Heidelberg, Germany*[a]
[17] *Institut für Reine und Angewandte Kernphysik, Universität Kiel, Kiel, Germany*[a]
[18] *Institute of Experimental Physics, Slovak Academy of Sciences, Košice, Slovak Republic*[f,j]
[19] *School of Physics and Chemistry, University of Lancaster, Lancaster, UK*[b]
[20] *Department of Physics, University of Liverpool, Liverpool, UK*[b]
[21] *Queen Mary and Westfield College, London, UK*[b]
[22] *Physics Department, University of Lund, Lund, Sweden*[g]
[23] *Physics Department, University of Manchester, Manchester, UK*[b]
[24] *CPPM, Université d'Aix-Marseille II, IN2P3-CNRS, Marseille, France*
[25] *Institute for Theoretical and Experimental Physics, Moscow, Russia*
[26] *Lebedev Physical Institute, Moscow, Russia*[f]

[27] *Max-Planck-Institut für Physik, München, Germany*[a]
[28] *LAL, Université de Paris-Sud, IN2P3-CNRS, Orsay, France*
[29] *LPNHE, Ecole Polytechnique, IN2P3-CNRS, Palaiseau, France*
[30] *LPNHE, Universités Paris VI and VII, IN2P3-CNRS, Paris, France*
[31] *Institute of Physics, Czech Academy of Sciences, Praha, Czech Republic*[f,h]
[32] *Nuclear Center, Charles University, Praha, Czech Republic*[f,h]
[33] *INFN Roma 1 and Dipartimento di Fisica, Università Roma 3, Roma, Italy*
[34] *Paul Scherrer Institut, Villigen, Switzerland*
[35] *Fachbereich Physik, Bergische Universität Gesamthochschule Wuppertal, Wuppertal, Germany*[a]
[36] *DESY, Institut für Hochenergiephysik, Zeuthen, Germany*[a]
[37] *Institut für Teilchenphysik, ETH, Zürich, Switzerland*[i]
[38] *Physik-Institut der Universität Zürich, Zürich, Switzerland*[i]
[39] *Institut für Physik, Humboldt-Universität, Berlin, Germany*[a]
[40] *Rechenzentrum, Bergische Universität Gesamthochschule Wuppertal, Wuppertal, Germany*[a]
[41] *Visitor from Physics Dept. University Louisville, USA*

[a] *Supported by the Bundesministerium für Bildung, Wissenschaft, Forschung und Technologie, FRG, under contract numbers 6AC17P, 6AC47P, 6DO57I, 6HH17P, 6HH27I, 6HD17I, 6HD27I, 6KI17P, 6MP17I, and 6WT87P*
[b] *Supported by the UK Particle Physics and Astronomy Research Council, and formerly by the UK Science and Engineering Research Council*
[c] *Supported by FNRS-NFWO, IISN-IIKW*
[d] *Partially supported by the Polish State Committee for Scientific Research, grant no. 115/E-343/SPUB/P03/120/96*
[e] *Supported in part by USDOE grant DE F603 91ER40674*
[f] *Supported by the Deutsche Forschungsgemeinschaft*
[g] *Supported by the Swedish Natural Science Research Council*
[h] *Supported by GA ČR grant no. 202/96/0214, GA AV ČR grant no. A1010619 and GA UK grant no. 177*
[i] *Supported by the Swiss National Science Foundation*
[j] *Supported by VEGA SR grant no. 2/1325/96*

1 Introduction

Intensity interferometry was first used in radio astronomy by Hanbury-Brown and Twiss (HBT-effect [1]) to measure the spatial extent of stars in 1953. In particle physics the HBT-effect was rediscovered in 1959 by G. and S. Goldhaber, Lee and Pais in antiproton-proton annihilation [2]. The GGLP effect, as it was called then, in its original form, described the tendency of pairs of like-sign pions to have smaller opening angles than pairs of unlike-sign pions. This effect was shown to arise from the symmetrisation of the wave functions of multi-boson states, hence is also known as Bose-Einstein correlation, and now normally refers to the enhanced probability for identical boson pairs to have similar momenta. The shape of the enhancement in relative momentum space was shown to be related to the spatial dimensions of the pion source. Bose-Einstein correlations (BEC) have since been studied in high-energy physics in nearly every type of reaction, e.g. in e^+e^- annihilation, in lepton nucleon (ℓN) scattering, in πN, KN, NN, and $\overline{N}N$ reactions, as well as in relativistic heavy-ion collisions with the aim of understanding the space-time evolution of the boson source. Many reviews of this subject exist [3–6]. In recent years it has been emphasized that Bose-Einstein correlations are but one of the many facets of multi-particle correlation studies (see e.g. [7,8] for a review). Independently of the details of the interpretation, the experimental study of BEC in a broad variety of reactions should eventually lead to better understanding of the space-time geometry of multihadron production [9].

1.1 Bose-Einstein correlations

Two-particle Bose-Einstein correlations are usually described in terms of normalized two-particle densities

$$R = \frac{P(1,2)}{P(1)P(2)} \ , \tag{1}$$

where $P(1,2)$ and $P(i)$ $(i = 1,2)$ are, respectively, the two-particle and single-particle inclusive densities. Bose-Einstein correlations show up as an enhancement in the production rate of identical pions with similar four-momenta, and reflect both geometrical and dynamical properties of the particle radiating source. If the particles are assumed to be emitted from a set of independently radiating sources distributed in space-time with a distribution $\rho(\xi)$, and the particles are identical bosons, imposing Bose symmetry on the production amplitude leads to a correlation function

$$R(T) = R_0(1 + \lambda \mid \tilde{\rho}(T) \mid^2) \ , \tag{2}$$

where $\tilde{\rho}$ is the Fourier transform of $\rho(\xi)$; R_0 is a normalisation constant and T is related to the invariant mass M of a pion pair with four-momenta p_1 and p_2 by

$$T^2 = -(p_1 - p_2)^2 = M^2 - 4m_\pi^2 \ . \tag{3}$$

The parameter λ in Eq. (2) is usually assumed to reflect the degree of incoherence of the source, i.e. $\lambda = 1$ for complete incoherence and $\lambda = 0$ for complete coherence. A static sphere of emitters with Gaussian density of the form

$$\rho(\xi) = \rho(0) \exp(-\frac{\xi^2}{2r^2}) \ , \tag{4}$$

where the parameter r corresponds to the size of the production volume, leads to a correlation function

$$R(T) = R_0(1 + \lambda \exp(-r^2 T^2)) \ , \tag{5}$$

usually referred to as Goldhaber parametrisation [3].

However, the simple geometrical interpretation of the interference pattern, based on an optical analogy is invalid when emitters move relativistically with respect to each other, leading to strong correlations between the space-time and momentum-energy coordinates of emitted particles [10, 11]. Correlations of this type arise due to the nature of inside-outside cascade dynamics [12] as in colour-string fragmentation [13]. In the interpretation of BEC by Andersson and Hofmann [14] and Bowler [11,15] in the string model, the length scale measured by BEC is therefore not related to the size of the total pion emitting source, but to the space-time separation between production points for which the momentum distributions still overlap. This distance is, in turn, related to the string tension. The model predicts an approximately exponential shape of the correlation function

$$R(T) = R_0(1 + \lambda \exp(-rT)) \ , \tag{6}$$

where r is expected to be independent of the total interaction energy.

In recent years, considerable experimental effort has been devoted to the study of fluctuation phenomena in multiparticle production processes [8]. These studies, complemented by theoretical analyses of the (approximately) self-similar character of perturbative QCD cascades, concentrated on the search for "intermittency": the occurrence of large fluctuations in particle density arising from scale-invariant dynamics. This work has provided firm indications that intermittency is strongly connected with Bose-Einstein correlations [8]. Scale invariance implies that multiparticle correlation functions exhibit power law behaviour over a considerable range of the relevant relative distance measure (such as T^2 or M^2) in phase space. As such, BEC from a static source do not exhibit power law behaviour. However, a power law is obtained if the size of the particle source fluctuates event-by-event, and/or, if the source itself is a self-similar (fractal-like) object extending over a large volume [16]. Power law behaviour of BEC has been observed in several experiments [17–19]. In these studies, the ratio R is parametrised using the form

$$R(M) = A + B \left(\frac{1}{M^2} \right)^{\beta} \ . \tag{7}$$

1.2 Outline

In this paper we analyse BEC in deep inelastic positron proton scattering (DIS) at HERA. The present study differs from previous studies of BEC in ℓN scattering [20–22] in several aspects. Since the data were taken at a tenfold higher centre of mass energy, they also cover a larger range in the kinematical quantities Bjorken$-x$ and momentum transfer Q^2 [23]. The correlations in the data can therefore be analysed separately as a function of x, Q^2, and hadronic centre of mass energy W. In addition diffractive and non-diffractive events can be distinguished.

At HERA about 10% of the deep inelastic scattering events exhibit a large region of rapidity in which there is no significant hadronic activity [24,25]. These events are usually attributed to diffractive processes and are well described by Monte Carlo simulations in which diffraction is modeled as deep inelastic positron pomeron scattering where the pomeron has partonic structure.

To the best of our knowledge, BEC have never been studied in diffractive processes. Although it is expected that the fragmentation mechanism in these events is similar to that in non-diffractive DIS, it nevertheless remains of interest to analyse BEC separately for that class of events.

Aside from comparing diffractive and non-diffractive samples, a specific goal of our analysis is to confront the correlation data with the different interpretations referred to above. In addition we use the Goldhaber parametrisation as a tool for the comparison with previous experiments.

This paper is organized as follows. After a brief presentation of the H1 detector, the event and track selections are described in Sect. 3. The Monte Carlo models used for comparison are listed in Sect. 4. The details of the analysis procedure and systematic uncertainties are given in Sect. 5. The results and conclusions are presented in Sect. 6 and Sect. 7, respectively.

2 The H1 detector

The data were taken with the H1 detector at the HERA ep – collider in 1994, with 27.5 GeV positrons colliding head-on with 820 GeV protons at a centre of mass energy $\sqrt{s} = 300$ GeV. A detailed description of the H1 detector can be found elsewhere [26]. Here we briefly describe the components relevant for this study.

The present analysis is based on the central tracking system, closest to the interaction point, and covering polar angles between 20° and 160°, where θ is defined with respect to the proton beam direction ($+z$ axis). Measurements of the charge and momentum of charged particles are provided by two large cylindrical drift chambers (central jet chambers, CJC1 and CJC2). The chambers have wires strung parallel to the beam axis ($z-$direction) with the drift cells inclined with respect to the radial direction, yielding up to 56 space points. The measured space point resolution in the drift coordinate ($r-\phi$ plane) is 170 μm and can, by comparing signals read out at both wire ends, achieve a resolution of one percent of the wire length in z. Two sets of thin cylindrical $z-$drift chambers complement the measurement of charged track momenta and are located at the inner radii of the jet chambers. The $z-$chambers provide track elements with typically 300 μm resolution in z and 8° in ϕ. This requires a drift direction parallel to, and sense wires perpendicular to, the beam axis. The central tracking system is complemented by a forward tracking system and a backward proportional chamber (BPC) covering the polar angle ranges $7° \leq \theta \leq 25°$ and $155° \leq \theta \leq 175°$, respectively. The BPC combined with a measurement of the interaction vertex position, is used to measure the polar angle of the scattered positron to better than 1 mrad.

Surrounding the tracking system is a liquid argon calorimeter consisting of electromagnetic and hadronic sections covering $4° \leq \theta \leq 153°$ over the full azimuth. Outside these detectors a superconducting coil provides a uniform magnetic field of 1.15 T parallel to the beam line. To measure the energy of the scattered positron, a backward electromagnetic calorimeter (BEMC) covers the angular range $155.5° \leq \theta_e \leq 174.5°$. Behind the BEMC is the time-of-flight system (ToF), consisting of two planes of scintillators, with a time resolution of 1 ns. It is used to reject events caused by the interaction of the proton beam with material before the detector. Such particles arrive at the ToF system before particles from the nominal interaction point. In the forward direction, surrounding the beam-pipe, is the plug, a copper/silicon calorimeter, covering the angular range $0.7° \leq \theta \leq 3.5°$. Further forward are the forward muon drift chambers on

either side of a toroidal magnet around the beam-pipe. Their primary purpose is to detect low angle muons, but they are also used to detect particles coming from secondary interactions with collimators designed to protect the detector from synchrotron radiation.

The most relevant performance parameters of the H1 detector for this analysis are the invariant mass resolution for charged particle pairs and the resolution of reconstructed event kinematics (for the latter see ref. [23]). The two-particle invariant mass resolution can be deduced from the widths of the K^0_S signal at $M = 0.5$ GeV and of the J/Ψ peak at $M = 3.1$ GeV to be $\sigma_M = 8.5$ MeV [27] and $\sigma_M = 76$ MeV [28], respectively. This agrees with Monte Carlo studies which also predict $\sigma_T = 3.5$ MeV at T=0.1 GeV.

3 Event and track selection

The present study is based on a sample of low Q^2 DIS events. The data sample comprises an integrated luminosity of 1.26 pb^{-1}. The scattered positron can be detected in the BEMC for Q^2 in the range from 1 GeV^2 to 100 GeV^2. The event selection used in this analysis follows closely that described in our structure function analysis [23]. In brief, the trigger used to collect low Q^2 data required a localised energy deposit in the BEMC of at least 4 GeV and no veto from the ToF system. This has been shown to be more than 99% efficient for the selection of DIS events in which the scattered positron entering the BEMC has an energy above 10 GeV.

3.1 Event selection

All events are required to have a vertex, reconstructed from tracks in the central tracker, located within $\pm$ 30 cm of the mean vertex z–position. This cut is required to reject beam–induced background and to permit a reliable determination of the kinematic variables. To exclude events with large QED radiative effects and to ensure substantial hadronic energy flow in the detector we require the invariant mass squared, W^2, of the hadronic system determined both with the Jacquet-Blondel method [29] and from the scattered positron to be larger than 4400 GeV^2, as well as the scattered positron to have an energy $E_e \geq 12$ GeV and a polar angle $157° \leq \theta_e \leq 172.5°$. The energy constraint ensures that the remaining photoproduction background is less than 1%. Finally, at least two selected tracks are required in each event irrespective of charge. This selection accepts events for Q^2 in the range $6 \leq Q^2 \leq 100$ GeV^2 and for x in the range $10^{-4} \leq x \leq 10^{-2}$. Both x and Q^2 are calculated from the positron nergy and angle.

The data are divided into diffractive and non-diffractive subsamples. Non-diffractive events are selected by requiring that the energy deposited in the liquid argon calorimeter within the polar angular range $4.4° \leq \theta \leq 15°$ be greater than 0.5 GeV. Diffractive events are selected by demanding that the energy deposited in the plug is less than 3 GeV, that there are fewer than three pairs of hits in the forward muon drift chambers, and that the most forward significant energy deposit (above 400 MeV) detected in the liquid argon calorimeter has a pseudo-rapidity of 3.0 or less. A further cut is made using the variable $x_{I\!P}$, defined as

$$x_{I\!P} = \frac{Q^2 + M_X^2}{Q^2 + W^2} \ , \tag{8}$$

where M_X^2 is the mass of the hadronic final state separated from the proton remnant system by

the largest rapidity gap [24]. In order to restrict the data to the kinematic region where pomeron exchange dominates and to ensure good acceptance of the dissociating pomeron-virtual boson system it is required that $x_{I\!P} \leq 0.05$. The quantity $x_{I\!P}$ can be interpreted as the fraction of the proton momentum carried by the pomeron.

After all cuts, the non–diffractive sample contains 48 000 events and the diffractive sample 2 500 events. The same selections are applied to the various Monte Carlo generated event samples used in the analysis. Further details are given in references [30, 31].

3.2 Track selection

Charged tracks are required to be linked to the primary event vertex and to show at least 10 hits within the jet chambers. Requiring a transverse momentum $p_t > 0.15$ GeV rejects tracks curving strongly within the CJC. A polar angle θ satisfying $22^\circ < \theta < 150^\circ$ restricts the analysis to particles which can be measured in both jet drift chambers in order to improve the quality of the tracks.

BEC studies are sensitive to double counting effects, i.e. the splitting of a single track into two pieces, which mimic two like-charge tracks with a very low value of T. In this experiment we find that tracks are split mainly between the inner and outer jet chamber. Thus only tracks which start within the inner CJC are considered. Monte Carlo studies have shown that this selection has a 95% track finding efficiency, and the remaining rate of split tracks is 0.3 %. This was verified by a visual scan of data. In addition no spurious tracks due to noise hits or reconstructed mirror hits of real tracks were found. To remove sensitivity to the remaining rate of split tracks all fits to the data are performed in the region $T > 0.018$ GeV. To further assess the quality of the simulation program, a comparison of track parameters between data and reconstructed Monte Carlo was made. Pairs with low invariant masses were selected both in data and in Monte Carlo and technical quantities such as radial track length, which is a good measure of track quality, were compared. Good agreement was found down to the lowest invariant mass included in this analysis.

All charged particles are assumed to be pions in this analysis. The effect of this assumption is discussed in Sect. 5.2. The influence of small differences in the reconstruction efficiency between positive and negative tracks due to the geometry of the jet chamber and a small torsion and consequent misalignment of the two jet chambers [32] were taken into account by separately analysing pairs of both charges. The effect on the results is described in Sect. 5.2 and found to be small.

4 Monte Carlo models

Non-diffractive neutral current DIS events are modelled using the Monte Carlo generator LEPTO [33, 34] which uses exact QCD matrix elements to first order to describe boson-gluon fusion, and QCD-Compton processes. Soft parton radiation is described by either the colour dipole model (CDM) [35] as implemented by ARIADNE 4.03 [36], in which the partons are radiated independently from a chain of dipoles, or the parton shower approach [37], where soft parton radiation is generated in the "leading log" approximation. The combination of matrix elements

with matched parton showers is referred to as the MEPS model [34], whilst combining matrix elements with CDM is referred to as MEAR and uses LEPTO 6.1 [33].

To study the effects of QED radiation the generator DJANGO 6.0 [38] is used which is an interface between HERACLES 4.4 [39] and LEPTO. It allows the inclusion of $\mathcal{O}(\alpha)$ processes including real photon emission from the positron as well as virtual electro-weak corrections.

The Monte Carlo generator RAPGAP 2.1 [40] is used to model diffractive DIS. The model uses parton density functions taken from leading order QCD fits to the measured diffractive structure function $F_2^{D(3)}$ [41]. As with LEPTO, exact matrix elements are used to calculate first order QCD radiation, with additional radiation incorporated using either CDM, or parton showers. In addition RAPGAP includes virtual QED effects to first order and real photon emission. The model employing RAPGAP with CDM is referred to as RAPA, and RAPGAP with parton showers is referred to as RAPP (Fig. 4).

All Monte Carlo generators used in this analysis employ the Lund string hadronisation model as implemented in JETSET 7.4 [42]. A method for the simulation of Bose-Einstein correlations is available as an option in the JETSET Monte Carlo [43]. The algorithm does not rigorously model BEC by symmetrising production amplitudes, but treats it as a final state interaction by reshuffling hadron momenta. As an option, the model assumes a Gaussian shape of the Bose-Einstein enhancement[1] according to the Goldhaber prescription of Eq. (5). This was used to generate a sample of non-diffractive DIS events referred to as MEAR(BEC). Unless stated otherwise, all Monte Carlo models refer to those without BEC simulated.

The H1 detector simulation program, H1SIM, is based on the CERN package GEANT [44] and was used to simulate the detector response in detail and to correct the data for geometrical acceptance, kinematical cuts, resolution and particle interactions with the detector material. The simulated events were processed through the same reconstruction chain as real data.

5 Analysis procedure

5.1 Construction of the correlation function

In order to measure the correlation function of Eq. (1) we normalize the two-particle like-sign inclusive density denoted by $\rho_2^l(T)$ to a reference sample $\rho^{ref}(T)$ which ideally contains no Bose-Einstein correlations and form the ratio

$$R(T) = \frac{\rho_2^l(T)}{\rho^{ref}(T)} , \quad \text{with} \quad \rho_2^l(T) \equiv \frac{1}{N}\frac{dn^{\pm\pm}(T)}{dT} \quad \text{and} \quad \int \rho_2^l(T)\, dT \equiv \langle n^l \rangle . \tag{9}$$

Here N is the total number of events, $n^{\pm\pm}(T)$ the number of $(++)$ and $(--)$ pairs in the sample, and $< n^l >$ is the mean number of like-sign pairs per event.

The choice of the reference sample is not trivial and has been a source of bias and systematic errors in all BEC measurements to date. Ideally it should satisfy the following conditions:

[1]The parameters $MSTJ(51)$ and $MSTJ(52)$ in the generator code were changed from their default values (see [42,43]) to 2 and 7, respectively. This choice leads to the inclusion of BEC for multi-pion and multi-kaon states with a Gaussian parametrisation, for which we have chosen $PARJ(92) = \lambda = 1$ and $PARJ(93) = (\hbar c/r) = 0.38$ GeV, for r=0.53 fm.

absence of BEC, presence of correlations due to the topology and the global properties of the events, and absence of dynamical correlations due to resonances not present in like-sign pairs. In this analysis we use either the two-particle unlike-sign inclusive distribution

$$\rho^{ref}(T) = \rho_2^u(T) \equiv \frac{1}{N}\frac{dn^{\pm\mp}(T)}{dT} \quad \text{with} \quad \int \rho_2^u(T)\, dT \equiv \langle n^u \rangle \ , \tag{10}$$

where $n^{\pm\mp}(T)$ is the number of $(+-)$ pairs in the sample, and $\langle n^u \rangle$ is the mean number of unlike-sign pairs per event, or we create uncorrelated pairs by mixing tracks from different events, denoted by

$$\rho^{ref}(T) = \rho_1 \otimes \rho_1(T) \ , \quad \text{normalized as} \quad \int \rho_1 \otimes \rho_1(T)\, dT = \langle n^l \rangle \ . \tag{11}$$

A mixed event is constructed by taking all combinations of each track in one event with all tracks in another event. In order to reduce statistical errors each event is mixed with 20 others.

We then define three ratios of densities as follows:

$$R^{lm} = \frac{\rho_2^l}{\rho_1 \otimes \rho_1} \ ; \qquad R^{um} = \frac{\rho_2^u}{\rho_1 \otimes \rho_1} \ ; \qquad R^{lu} = \frac{\rho_2^l}{\rho_2^u} \ . \tag{12}$$

The same techniques were commonly used in the past in many experiments [17,18,20,21,45–49], but for each experiment special treatment is necessary.

At HERA, events are observed in a wide range of virtual-photon proton ($\gamma^* p$) centre of mass energies, and hence the data sample comprises quite different topologies depending on the position of an event in the $x - Q^2$ plane. Events with large Q^2 on average have a current (struck quark) system which is boosted further forward in the laboratory system than events at lower Q^2. Event topologies as seen in the transverse $(r - \phi)$ plane have a hadronic system which is balanced against the scattered lepton. Mixing tracks from events with non-collinear hadronic systems, would yield track pairs with artificially large momentum differences. Thus, in order to overcome this bias, all events are rotated in the $r - \phi$ plane such that the positron has $\phi = 0$. A similar effect is expected to hold in the $\theta - z$ plane. However, this effect can be reduced by mixing events with similar Q^2 and W values. Mixed events are, therefore, required to differ in Q^2 by not more than 20 GeV^2, and in W by less than 20 GeV. The difference in event charged multiplicity was restricted to be less than three.

The unlike-sign, like-sign and event-mixed densities constructed from our data are shown for the non-diffractive sample in Fig. 1a and for the Monte Carlo simulations in Fig. 1b. Since the standard Monte Carlo simulation does not include BEC, the like-sign pair distribution constitutes, in principle, the ideal reference distribution for a Monte Carlo with BEC included (shown as stars in Fig. 1b). Neither the mixed-event nor the unlike-sign reference distribution from data is consistent with ρ_2^l obtained from the Monte Carlo model without BEC.

Mixing tracks from different events apparently shifts the distribution towards larger T compared to the invariant mass distribution of the same event, as we can deduce by comparing $\rho_1 \otimes \rho_1(T)$ with $\rho_2^l(T)$, both shown in Fig. 1b. We therefore conclude that despite the precautions taken in constructing it, the mixed-pair sample still differs from the ideal reference distribution in the topological, momentum and charge conservation constraints.

The unlike-pair distribution ρ_2^u contains dynamical correlations from K_S^0 and resonance decays, most notably from the ρ^0, η, η', and ω. A sharp peak at $T \simeq 0.4$ GeV can be seen in

ρ_2^u (Fig. 1a) which arises from the K_S^0 and the broad maximum at $T \simeq 0.7$ GeV stems from the ρ^0 decay. The contributions from η, η', and ω decay do not appear as sharp peaks and are more troublesome for the analysis than those from K_S^0 and ρ^0, because they contribute to the low mass region, where BEC appear. To illustrate this we have used the Monte Carlo model to display the contributions from resonance decays in Fig. 2a. The K_S^0 (not shown) and ρ^0 decays cluster in a sufficiently narrow mass region, and are removed by excluding the regions $0.37 - 0.43$ GeV (K_S^0) and $0.65 - 0.85$ GeV (ρ^0) in T from the analysis.

The ratio of the data to the MEAR(BEC) model shown in Fig. 1c decreases smoothly with T for both ρ_2^u and ρ_2^l. Distinct dips or peaks are not observed in either the low mass, the K_S^0 or the ρ^0 region. A smooth T dependence is also observed for the ratio of the density for pion pairs to the density for all charged particle pairs. This ratio was obtained within the MEAR Monte Carlo model and is shown in Fig. 2b.

The shortcomings of the reference distributions constructed from the data can be corrected, to first order, if both the correlated and uncorrelated distributions are divided by the corresponding Monte Carlo distributions. Thus in order to discriminate BEC from other dynamical correlations, we consider a double ratio by dividing the correlation function of Eq. (9) obtained from the data, by that obtained from reconstructed Monte Carlo events which do not contain BEC:

$$RR(T) = \frac{R^{data}(T)}{R^{MC}(T)} \; . \tag{13}$$

This procedure should also correct for the detector acceptance, analysis cuts and the lack of particle identification provided that the Monte Carlo simulation can represent the observed distributions sufficiently well, as we will show in Sect. 6.1. The double ratio is then fitted with a modified version of Eq. (5) or Eq. (6) in order to extract the parameters r and λ for the Gaussian and the exponential parametrisations:

$$RR(T) = \quad R_0(1 + aT)(1 + \lambda \exp(-r^2T^2)) \; , \tag{14}$$

$$RR(T) = \quad R_0(1 + aT)(1 + \lambda \exp(-rT)) \; . \tag{15}$$

Here R_0 is a global normalization factor, and the additional parameter a allows for remaining long-range correlations.

5.2 Systematic errors and corrections

To verify the stability of our results with respect to the assumptions made concerning the reference distributions, and to estimate the systematic errors arising from experimental resolutions and the treatment of the data, we have performed a number of checks described in the following. In order to quantitatively assess the influence of an assumption or a particular analysis step, the deviations of the parameter values relative to that of the reference fit are determined. The reference fit uses Eq. (14) for the Gaussian parametrisation, and Eq. (15) and Eq. (7) for the exponential and power law fits, respectively. The MEAR Monte Carlo is used to calculate the double ratios, and the fit to the non-diffractive data is performed in the range from 0.018 to 2 GeV in T (0.018 to 1.0 GeV in T for power law fits) and to the diffractive data in the range from 0.036 to 2 GeV. For the unlike-sign reference distribution, the regions of the ρ^0 resonance

and the K^0_S are excluded from the fit (see Sect. 5.1). The observed deviations from the reference fit are then considered in the evaluation of the systematic error.

We first discuss those checks which use Monte Carlo events only, and where we study the influence of reference sample choice and detector effects.

Reference sample: The systematic effects associated with the choice of the reference sample can be studied "in Monte Carlo only" experiments using MEAR(BEC) treated as "data". MEAR without BEC is used for the denominator of the double ratios. This can be done at both the reconstructed level, i.e. after full detector simulation and reconstruction, and at the generator level. In addition, the like-sign density from MEAR without BEC may be used ideally in the denominator for $R(T)$ in Eq. (9), with ρ^l_2 in the numerator obtained from the MEAR(BEC) Monte Carlo model. In this case the single ratio ρ^l_2(MEAR(BEC))/ρ^l_2(MEAR) is fitted with the standard Gaussian parametrisation (Eq. (14)). The results are given in Table 1 and show that a fit using the ideal reference distribution is able to reproduce the input value for r (0.53 fm) within the statistical errors. The results of fits to the double ratios RR^{lm} and RR^{lu} are also given in Table 1. Inspection of these results reveals, not unexpectedly (see Sect. 5.1 above), that neither the use of the unlike-sign nor the event-mixed reference distribution can reproduce Monte Carlo input values, not even at the generator level. The shift towards larger radii, between 0.18 fm for unlike-sign pairs and 0.08 fm for event-mixing is significant, and could, in principle, be used to correct the experimental results. We have not applied such a correction to allow comparison with other experiments (Sect. 6.3) which have observed this shift, but have not corrected for it.
The value extracted for λ (0.38) differs from the input value ($\lambda = 1$), since resonance decay products and charged particles other then pions are not distinguished when constructing the correlations. It is with respect to this value, that we must evaluate further differences introduced by the choice of the reference sample. Table 1 shows that these are sizeable. For this reason, the values of λ found by different experiments, and in different reactions, differ significantly and it seems hazardous to draw definitive conclusions from such comparisons.

Detector Effects: Finite detector resolution and acceptance as well as imperfect pattern recognition in the reconstruction step can influence the BEC analysis. As Table 1 shows the difference in the extracted parameters between generator and detector level for the radius parameter is small, though clearly noticeable for λ. This comparison is repeated for all sets of low Q^2 non-diffractive data discussed below separately and included as a contribution to the systematic error.

The following contributions to the systematic error are evaluated from the data directly.

Models: To assess the model dependency of the results we utilize both the MEAR and MEPS Monte Carlo models for the construction of the acceptance corrected double ratios.

Background parametrisation: As alternatives to the linear parametrisation of long-range correlations used in our reference fits (Eq. (14) and Eq. (15)) we used the following forms

$$RR(T) = \quad R_0(1 + aT + \epsilon T^2)(1 + \lambda \exp(-r^2T^2)) \ , \tag{16}$$

Monte Carlo Level	Reference samples					
	like-sign $\rho_2^l(T)$		unlike-sign RR^{lu}		event-mixed RR^{lm}	
	r(fm)	λ	r(fm)	λ	r(fm)	λ
GEN	0.51 ± 0.02	0.38 ± 0.02				
REC			0.67 ± 0.04	0.48 ± 0.04	0.61 ± 0.04	0.28 ± 0.02
GEN			0.71 ± 0.04	0.57 ± 0.04	0.61 ± 0.03	0.35 ± 0.02

Table 1: Gaussian fit results (Eq. (14)) using MEAR(BEC) Monte Carlo (see Sect. 4) treated as "data". The input parameters for MEAR(BEC) were $r = 0.53$ fm, and $\lambda = 1$. MEAR without BEC is used as the denominator for construction of the double and single ratios. The entries "GEN" and "REC" refer to using the Monte Carlo before and after the detector simulation and reconstruction step. Results from fits to the single ratio are given in the column labeled ρ_2^l. Results from fits to the double ratios RR^{lm} and RR^{lu} are given in the last two columns.

$$RR(T) = \quad R_0(1 + aT + \epsilon T^2)(1 + \lambda \exp(-rT)) \ . \tag{17}$$

Assuming that the uncorrelated background is constant over the full range in T, as in Eq. (5) and Eq. (6), leads to worse values of χ^2 in most cases, and hence is not considered. We also repeated all Gaussian and exponential fits with an upper limit in T of 1.2 GeV instead of 2 GeV. For the power law fit (Eq. (7)) the upper limit was increased to 1.2 GeV.

Charge sign: Differences in the detector response to positively and negatively charged particles could cause systematic shifts of the data. Therefore we analysed positive and negative pairs separately to assess the influence of such effects. For the diffractive data we have assumed the same error as for the non-diffractive sample, since further splitting of an already statistically small sample would lead to statistical errors far exceeding the systematic effect we were studying.

Data treatment: Technical changes such as bin width, track selection criteria, and the influence of the resonances (including the K_S^0 and ρ^0 mass region for the unlike-sign reference sample) were investigated and found to have no influence outside statistical fluctuations. In addition the restriction $T > 0.018$ GeV was raised to 0.036 GeV and led to negligible changes in all fit parameters.

Event-mixing: The analysis was repeated using a simpler method of event-mixing whereby the data sample was subdivided into four W classes and each event was mixed with one other event within the same class. In this analysis a less restrictive W^2 selection (as determined via the Jacquet-Blondel method) was used, in addition to an alternative track selection. The two analyses are in good agreement with each other [30]. Furthermore, the analysis of the diffractive data was repeated with more stringent restrictions on the mixing of events. Specifically, the requirements were tightened to $\Delta W < 10$ GeV, and $\Delta Q^2 < 10$ GeV^2. This was also found to have no influence on the results [31].

Final-state interactions: We have not applied corrections for electromagnetic [50, 51] and strong [52] $\pi\pi$ interactions in the final state to the data, or for the purity of the pion sample, as e.g. done by the DELPHI-collaboration [17]. We calculated the Coulomb corrections and found that they affect only the region $T < 0.05$ GeV, changing λ and r by

$\delta\lambda = 0.03$ and $\delta r = 0.02$ fm, respectively. A purity correction in the sense, that one tries to correct the observed distribution eliminating decay products from long-lived resonances and charged particles other than pions, can be made by rescaling the data using the ratio of pions, which are either directly produced or decay products of short lived resonances, to that of all charged particles given by the Monte Carlo models. Using this procedure we have confirmed the observations of the DELPHI-collaboration [17], that only changes in the radius parameter of about 1σ (statistical) are observed, whilst λ becomes consistent with one (see [30,31]).

QED radiation: QED effects were investigated using the Monte Carlo model DJANGO [38] and found to be negligible for the ratios used in the analysis [31].

The most important contributions to the systematic errors for diffractive and non-diffractive data are given in Table 2 and Table 3, and are added in quadrature for the final errors quoted. For the exponential and power law parametrisations (Eq. (15) and Eq. (7)) the corresponding systematic uncertainties are listed in Table 4 and Table 5. When using the preferred event-mixed technique, the systematic errors of r are sufficiently small to allow a meaningful comparison with other experiments and between different subsets of our data. However, since systematic uncertainties in the determination of λ are as large as 60% in some cases, and λ is also very sensitive to pion purity, we place no emphasis on our measurement of λ, but include results in the following for completeness.

	unlike-sign $\rho_2^u(T)$		event-mixed $\rho_1 \otimes \rho_1(T)$	
	δr(fm)	$\delta\lambda$	δr(fm)	$\delta\lambda$
Detector effects	-0.04	-0.09	± 0.00	-0.06
Background parametrisation	-0.01	$+0.01$	$+0.02$	± 0.00
Models	± 0.02	± 0.19	± 0.00	± 0.06
Track charge	± 0.01	± 0.01	± 0.02	± 0.02
Sum	$+0.02$	$+0.19$	$+0.03$	$+0.06$
(quadratic)	-0.05	-0.21	-0.02	-0.09
Reference sample †	$+0.18$	$+0.19$	$+0.08$	-0.03
Statistical error	± 0.04	± 0.03	± 0.03	± 0.02

Table 2: Contributions to the systematic errors for the non-diffractive data sample and the Gaussian parametrisation (Eq. (14)). The last row shows the statistical error obtained from the reference fit for comparison. † Observed shift in the Monte Carlo extracted parameters compared to a like-sign reference distribution without BEC (see text and Table 1).

6 Results

6.1 Comparison of the data with Monte Carlo predictions

In Figs. 3, 4 and 5 we examine how well the data are described by the Monte Carlo simulations. From the ratio $R^{um}(T)$ shown in Fig. 3a for data, MEAR and MEPS Monte Carlo we can infer

	unlike-sign $\rho_2^u(T)$		event-mixed $\rho_1 \otimes \rho_1(T)$	
	δr(fm)	$\delta\lambda$	δr(fm)	$\delta\lambda$
Background parametrisations	± 0.04	$+0.23$	± 0.01	$+0.13$
Models	± 0.03	± 0.11	± 0.01	± 0.08
Track charge	± 0.01	± 0.01	± 0.02	± 0.02
Sum	$+0.05$	$+0.26$	$+0.02$	$+0.15$
(quadratic)	-0.05	-0.11	-0.03	-0.08
Statistical error	± 0.13	± 0.13	± 0.06	± 0.08

Table 3: Contributions to the systematic errors for the diffractive data sample using the Gaussian parametrisation (14). The statistical error is that obtained from the reference fit.

	unlike-sign $\rho_2^u(T)$		event-mixed $\rho_1 \otimes \rho_1(T)$	
	δr(fm)	$\delta\lambda$	δr(fm)	$\delta\lambda$
Detector effects	$+0.02$	$+0.15$	-0.04	$+0.11$
Background parametrisation	-0.27	$+0.54$	$+0.08$	-0.09
Models	± 0.04	± 0.38	± 0.04	± 0.12
Track charge	± 0.01	± 0.02	± 0.03	± 0.05
Sum	$+0.05$	$+0.68$	$+0.09$	$+0.17$
(quadratic)	-0.27	-0.38	-0.06	-0.16
Statistical error	± 0.09	± 0.08	± 0.11	± 0.06

Table 4: Contributions to the systematic errors for the non-diffractive data sample using an exponential parametrisation (15). The statistical error is that obtained from the reference fit.

	unlike-sign $\rho_2^u(T)$			event-mixed $\rho_1 \otimes \rho_1(T)$		
	$\delta\beta$	δB	δA	$\delta\beta$	δB	δA
Detector effects	-0.01	-0.001	-0.01	-0.09	$+0.006$	-0.01
Background parametrisation	$+0.29$	-0.002	$+0.02$	$+0.12$	-0.005	-0.01
Models	± 0.30	± 0.003	± 0.03	± 0.08	± 0.003	± 0.00
Track charge	± 0.15	± 0.003	± 0.00	± 0.04	± 0.001	± 0.00
Sum	$+0.44$	$+0.004$	$+0.04$	$+0.15$	$+0.007$	$+0.00$
(quadratic)	-0.34	-0.005	-0.03	-0.13	-0.006	-0.01
Statistical error	± 0.20	± 0.002	± 0.01	± 0.15	± 0.006	± 0.01

Table 5: Contributions to the systematic errors for the non-diffractive data sample using a power law parametrisation (7). The statistical error is that obtained from the reference fit.

that the fragmentation model (JETSET) seems to overestimate the amount of ρ^0 production, as previously observed [17, 18, 45, 53]. However, as no such discrepancy is seen in Fig. 1c, we conclude that the inclusion of BEC in Monte Carlo models is able to satisfactorily describe the ρ^0 production region. The Monte Carlo also fails to predict correctly the T region ($0.1 < T < 0.2$ GeV), where reflections of the η, ω and η' resonances appear (Fig. 3a). At the smallest values of T a sharp spike (truncated in the figures) can been seen in Fig. 3a and Fig. 3b. For like-sign pairs this is attributed to the residual effects of track double counting. Similarly, photons converting into e^+e^- pairs contribute to the first bin in the unlike-sign pair distributions. Good agreement between data and Monte Carlo model is observed in the lowest bin (not visible in Figs. 3a and 3b).

In Figs. 3b, 3c, 4b and 4c the Bose-Einstein enhancement is clearly visible for like-sign pairs for $T < 0.4$ GeV in the ratios R^{lm} and R^{lu}. The slow rise of R^{lm} towards threshold, predicted by the models, is caused by mixing tracks of events with a different topology as discussed in Sect. 5.1 and in [17, 45]. At larger T the Monte Carlo models give a good description of the data. The K^0_S and ρ^0 signals are visible as distinct dips in Fig. 3c.

In Fig. 5a we compare the ratio R^{um} for non-diffractive data with the MEAR(BEC) Monte Carlo simulation. Apart from the very low T region, good agreement is seen. Figure 5b shows the ratio R^{lm}. Since the radius r used in the generation step lies close to the experimental result, this model provides a rather accurate representation of the data except for $T < 0.2$ GeV where the data systematically exceed the prediction. This gives evidence that the Bose-Einstein enhancement rises somewhat faster towards threshold than expected from a Gaussian parametrisation of the correlation function. This was noticed in previous experiments (see e.g. [22, 49, 53, 54]).

6.2 Fits to the measured distributions

6.2.1 BEC in diffractive and non-diffractive DIS

Figures 6 and 7 show the data, from which our final results are derived and which serve as reference plots for the discussion of the systematic errors in Sect. 5.2. The results from the fits to these double ratios using the Goldhaber parametrisation (Eq. (14)) are superimposed on the data. Table 6 summarises the results, which were obtained in this analysis using the non-diffractive and diffractive data sets, for both the event-mixed and unlike-pair reference samples. The parameter a (typically between 0.01 to 0.02 GeV^{-1}) has been omitted (see Eqs. (14) – (15)).

As seen from Table 6, the BEC parameters derived from the event-mixed and from the unlike-sign reference samples differ substantially. This was also observed in many earlier experiments [17, 20, 21, 45, 55, 56], and subsequently ascribed [4, 57] to correlations due to the production of long-lived resonances and $\pi\pi-$interactions in the final state, as we have discussed above. This observation is independent of the choice of the Monte Carlo generator used to describe the scattering process. The difference appears already at the generator level, in the double and single ratios as is apparent from Table 1. The event-mixing method, however, leads to values of r which are in closer agreement with the input value used in the Monte Carlo generator with BEC.

The data in Table 6 provide no evidence for a statistically significant difference between

Data set	event-mixed $\rho_1 \otimes \rho_1(T)$		
	r (fm)	λ	χ^2/ndf
non-diffractive	$0.54 \pm 0.03\ ^{+0.03}_{-0.02}$	$0.32 \pm 0.02\ ^{+0.06}_{-0.09}$	96/72
diffractive	$0.49 \pm 0.06\ ^{+0.02}_{-0.03}$	$0.46 \pm 0.08\ ^{+0.15}_{-0.08}$	18/23
Data set	unlike-sign $\rho_2^u(T)$		
	r (fm)	λ	χ^2/ndf
non-diffractive	$0.68 \pm 0.04\ ^{+0.02}_{-0.05}$	$0.52 \pm 0.03\ ^{+0.19}_{-0.21}$	77/56
diffractive	$0.59 \pm 0.13\ ^{+0.05}_{-0.05}$	$0.46 \pm 0.13\ ^{+0.26}_{-0.11}$	26/17

Table 6: Summary of experimental results for the Gaussian fits (Eq. (14)) to the two data samples using both types of reference distributions. The first error is statistical, the second is systematic.

the BEC parameters in predominantly non-diffractive and diffractive DIS interactions. The observation of similar BEC effects supports the idea that the basic fragmentation mechanism is similar for diffractive and non-diffractive events.

When comparing with other experiments, or searching for dependencies on kinematic quantities such as x, Q^2, W, or multiplicity, we concentrate in the following on the statistically more significant non-diffractive data set.

6.2.2 Kinematical and multiplicity dependence of BEC

In order to study BEC under different conditions, the non-diffractive data sample is divided into three classes for the three kinematic variables separately, as listed in Table 7. The double ratio correlation functions $RR(T)$ are constructed with the mixed-event reference sample and then fitted to Eq. (14). The results are summarised in Table 7. The parameters are found, within the statistical errors, to be independent of the kinematical region considered.

	r(fm) λ	r(fm) λ	r(fm) λ
x	0.60±0.06 0.30±0.03	0.56±0.05 0.34±0.03	0.44±0.06 0.38±0.07
	$(0.0001 \leq x < 0.0006)$	$(0.0006 \leq x < 0.0019)$	$(0.0019 \leq x < 0.01)$
Q^2 (GeV^2)	0.52±0.04 0.42±0.04	0.63±0.08 0.25±0.04	0.47±0.04 0.41±0.05
	$(6 \leq Q^2 < 12)$	$(12 \leq Q^2 < 25)$	$(25 \leq Q^2 \leq 100)$
W (GeV)	0.52±0.07 0.26±0.05	0.48±0.03 0.42±0.04	0.68±0.08 0.34±0.04
	$(65 \leq W < 120)$	$(120 \leq W < 180)$	$(180 \leq W < 240)$

Table 7: Parameters r and λ extracted using Eq. (14) for each subset of the non-diffractive data sample. Only statistical errors are given.

We have also grouped the non-diffractive data into three subsets of observed charged particle multiplicity. Figure 8 shows the corresponding experimental distributions and fits. The classes and the corresponding values found for r and λ are listed in Table 8. The value of the parameter r is observed to rise with increasing multiplicity. Indications for an opposite trend are noticeable

for x. Previously we have observed that the multiplicity is nearly independent of Q^2, but depends weakly on W [58]. The kinematical relation $Q^2 \sim xW^2$, at small x, leads one then to expect a positive correlation of r with W and a negative correlation with x, if r increases with multiplicity. The data appear consistent with this expectation, though the effect is not significant in view of the statistical errors.

For each bin of observed multiplicity we determine the corrected true mean multiplicity using the iterative matrix migration method of reference [58]. The corrected mean charged particle densities are given in Table 8. The $\gamma^* p$ centre of mass pseudo-rapidity interval, as determined by our track selection criteria, is $\Delta\eta^* = 3.2$ ($1.1 < \eta^* < 4.3$).

In order to assess the significance of the observed increase of r with multiplicity, we repeat the systematic error analysis described in Sect. 5.2 for each multiplicity bin. The influence of the shape of the background slope at large T is such that the systematic uncertainty (see Table 8) is twice as large as the statistical errors, and hence the rise consistent with zero. For comparison with recent e^+e^- data [59] we have repeated the analysis with the unlike-sign reference sample, and also find a value for the slope statistically consistent with zero.

Observed Multiplicity	Corrected Multiplicity	event-mixed $\rho_1 \otimes \rho_1(T)$ r(fm) λ	unlike-sign $\rho_2^u(T)$ r(fm) λ
$4 \le n < 7$	$4.9 \pm 1.1^\dagger$	0.42±0.05 0.37±0.05	0.53±0.06 0.54±0.08
$7 \le n < 12$	$8.2 \pm 1.6^\dagger$	0.58±0.05 0.31±0.03	0.77±0.07 0.54±0.06
$n \ge 12$	$13.6 \pm 2.4^\dagger$	0.81±0.12 0.42±0.07	0.72±0.09 0.65±0.09
Slope		event-mixed $\rho_1 \otimes \rho_1(T)$	unlike-sign $\rho_2^u(T)$
$\frac{1}{<r>}\frac{dr}{dn}$		$0.085 \pm 0.026\ ^{+0.057}_{-0.048}$	$0.045 \pm 0.023\ ^{+0.069}_{-0.071}$
$\frac{1}{<\lambda>}\frac{d\lambda}{dn}$		$0.009 \pm 0.018\ ^{+0.048}_{-0.043}$	$0.024 \pm 0.026\ ^{+0.024}_{-0.054}$

Table 8: Parameters r and λ extracted using Eq. (14) for different multiplicity subsets of the non-diffractive data sample. The last two rows list the result for the relative slope of the two parameters with respect to charged multiplicity. The first column indicates the interval in observed multiplicity, the second column the corresponding corrected mean multiplicty. The first error quoted is statistical, and where given, the second is systematic. † These numbers are not errors, but represent the spread in true charged multiplicity in each subset.

6.2.3 Alternative parametrisations of BEC

Figure 9 shows the non-diffractive data of Fig. 6 together with the results from fits using the exponential, power law, and Gaussian parametrisations of Eq. (15), Eq. (7), and Eq. (14), respectively. The parameters for the fits are listed in Table 9. The quality of the fit for the exponential is slightly better than for the Gaussian parametrisation (χ^2/ndf= 85/72 compared to 96/72) and confirms previous observations (see e.g. [22]) that the Bose-Einstein correlation

function is decreasing faster with T than a Gaussian.

The power law form for the two-particle correlation function was originally suggested in the framework of a Mueller-Regge analysis of multiparticle inclusive spectra where the invariant mass occurs as a natural variable [60]. In recent studies of the intermittency effect, and its relation to BEC, power law behaviour for like-sign particle pairs was observed in hadron-hadron collisions [18] and e^+e^- annihilation at LEP [17] with values for the slope β close to 1.5. From Fig. 9 and Table 9 it is seen that a scale-invariant form of BEC provides a valid alternative parametrisation of the Bose-Einstein effect. In addition we find that fitting the power law over the range $0.018 < T < 2.0$ GeV, and using the fit function

$$RR(M) = A + \epsilon \cdot M + B \left(\frac{1}{M^2}\right)^{\beta} \quad , \tag{18}$$

which has an additional term linear in M with coefficient ϵ as a free parameter, we are able to obtain good fits over the range $1 < T < 2$ GeV, too. These result in a reduction of β to 0.91 ± 0.18 with χ^2/ndf=86/72 for RR^{lm}, and $\beta = 1.49 \pm 0.19$ with χ^2/ndf=80/56 for RR^{lu}.

Power law	β	B [GeV^{-2}]	A	χ^2/ndf
RR^{lm}	$1.20 \pm 0.15\ ^{+0.15}_{-0.13}$	$0.018 \pm 0.006\ ^{+0.007}_{-0.006}$	$0.93 \pm 0.01\ ^{+0.00}_{-0.01}$	49/49
RR^{lu}	$1.82 \pm 0.20\ ^{+0.44}_{-0.34}$	$0.005 \pm 0.002\ ^{+0.004}_{-0.005}$	$0.94 \pm 0.01\ ^{+0.04}_{-0.03}$	52/33
Exponential	a [GeV^{-1}]	r [fm]	λ	χ^2/ndf
RR^{lm}	0.08 ± 0.04	$0.68 \pm 0.11\ ^{+0.09}_{-0.06}$	$0.64 \pm 0.06\ ^{+0.17}_{-0.16}$	85/72
RR^{lu}	0.13 ± 0.02	$0.99 \pm 0.09\ ^{+0.05}_{-0.27}$	$1.00 \pm 0.08\ ^{+0.68}_{-0.38}$	85/56
Gaussian	a [GeV^{-1}]	r [fm]	λ	χ^2/ndf
RR^{lm}	0.02 ± 0.01	$0.54 \pm 0.03\ ^{+0.03}_{-0.02}$	$0.32 \pm 0.02\ ^{+0.06}_{-0.06}$	96/72
RR^{lu}	0.08 ± 0.02	$0.68 \pm 0.04\ ^{+0.02}_{-0.05}$	$0.52 \pm 0.03\ ^{+0.19}_{-0.21}$	77/56

Table 9: Results from the fits to the double ratios $RR^{lm}(T)$ and $RR^{lu}(T)$ from the non-diffractive data with a Gaussian (Eq. (14)), exponential (Eq. (15)) and power law (Eq. (7)) parametrisation. Where given, the first error is statistical, the second systematical.

6.3 Comparison with other experiments

Table 10 summarises the Gaussian fit results from other experiments for comparison with the present analysis. For completeness also results are included, which used correction methods different from ours, e.g. those where purity or Coulomb corrections were applied. These corrections mainly influence the parameter λ, which may explain the larger differences observed here. The values of r extracted with a mixed-event reference sample are systematically lower than those obtained with an unlike-sign reference, consistent with our data. However, when allowance is made for systematic errors, which not all experiments have quoted, but which are likely to be of similar size to ours, the measured radii are relatively consistent with each other. The fact that the data from $\ell N-$scattering are independent of the energy, and furthermore agree with those from e^+e^- annihilation at various centre of mass energies (with the exception of the MARK II - data [62]), seems to lend support to the string model interpretation, where the source dimension is related to the string tension and is energy independent.

The multiplicity dependence has also been studied in a few experiments. In e^+e^- annihilation at LEP [59] a small rise of r with observed multiplicity has been reported by OPAL, while λ was seen to decrease:

$$\frac{1}{< r >}\frac{dr}{dn} \;=\; 0.0036 \;\pm\; 0.0006 \;, \qquad \frac{1}{< \lambda >}\frac{d\lambda}{dn} \;=\; -\,0.0042 \;\pm\; 0.0008 \;.$$

The unlike-sign reference sample was used. Our values for this reference sample,

$$\frac{1}{< r >}\frac{dr}{dn} = 0.045 \pm 0.023 \;, \qquad \frac{1}{< \lambda >}\frac{d\lambda}{dn} = 0.024 \pm 0.026 \;,$$

are consistent with these results, albeit within large errors.

It may be argued that a more appropriate comparison is to examine the slopes with respect to mean particle density per interval of pseudorapidity rather then per interval of multiplicity, because the angular acceptance of the LEP experiments is different in the centre of mass system and the total multiplicity larger ($10 < n < 40$). We have scaled the e^+e^- results by the range in η^* accessible to OPAL ($\Delta\eta^* = 2$ and $\mid \eta^* \mid < 1$) and also our data by $\Delta\eta^*$ to obtain:

$$\frac{1}{< r >}\frac{dr}{d(dn/d\eta^*)} = 0.0072 \;\pm\; 0.0012 \;(\mathrm{OPAL}) \;, \quad \frac{1}{< r >}\frac{dr}{d(dn/d\eta^*)} = 0.144 \;\pm\; 0.074^{+0.220}_{-0.227} \;(\mathrm{H1}) \;.$$

The two data sets are still consistent.

In proton-proton and proton-antiproton collisions, first indications for a multiplicity dependence were seen at low centre of mass energies at the ISR [63]. Both the UA1-collaboration [64] at centre of mass energies between 200 and 900 GeV ($\mid \eta^* \mid < 3$) as well as the E735-collaboration [65] at 1.8 TeV ($\mid \eta^* \mid < 3.25$) report a strong increase of radius with particle density, $dn/d\eta^*$, in $\bar{p}p$ collisions. Figure 10 shows the results on r, together with our data converted into particle density, where all data were obtained using event-mixed reference samples. For UA1 we have only plotted the statistically most significant data set at 630 GeV. Our results match these data at the lower end reasonably well.

7 Conclusions

We have presented a study of Bose-Einstein correlations (BEC) at the highest centre of mass energy for $ep-$collisions available so far. Even at this high energy (300 GeV) the apparent source dimensions, measured by the width of the BEC signal are in good agreement with data from ℓN scattering at lower energies (10 to 30 GeV) and with most data from e^+e^- reactions between $\sqrt{s} = 29$ and $\sqrt{s} = 91$ GeV. BEC in diffractive DIS have been measured for the first time, and no difference between diffractive and non-diffractive data has been observed. No Q^2, x or W dependence is observed in the kinematical ranges accessible at HERA. These observations fit well within the picture inherent to string models, that hadronisation is a universal phenomenon and that the measured spatial dimensions reflect mainly the constant string tension.

For the non-diffractive data, where statistics are highest, we have examined alternative parametrisations of the Bose-Einstein correlation function. Both an exponential form in T and a power law in invariant mass describe the Bose-Einstein enhancement at threshold well. The

Experiment	unlike-sign $\rho_2^u(T)$		event-mixed $\rho_1 \otimes \rho_1(T)$	
$\sqrt{s}$, W [GeV]	r(fm)	λ	r(fm)	λ
e^+e^-				
DELPHI [55]	0.83±0.03	0.31±0.02	0.47±0.03	0.24±0.02
91	(0.82±0.03)	(0.45±0.02)	(0.42±0.04)	(0.35±0.04)
DELPHI [17]			(0.49±0.01±0.05)	(1.06±0.05±0.16)
ALEPH [45]	0.82±0.04	0.48±0.03	0.52±0.02	0.30±0.01
91	(0.82±0.04)	(0.62±0.04)	(0.50±0.02)	(0.40±0.02)
OPAL [59]	0.955±0.012±0.015	0.672±0.013±0.024		
91				
AMY [47]	0.73±0.05±0.20	0.47±0.05±0.05	0.58±0.06±0.02	0.39±0.04±0.03
58				
TASSO [61]	0.82±0.06±0.04	0.35±0.03		
34	(0.80±0.06±0.04)	(0.70±0.06±0.09)		
MARK II† [62]	0.75±0.03±0.04	0.28±0.02±0.04	0.97±0.10±0.05	0.27±0.04±0.02
29	(0.84±0.06±0.05)	(0.50±0.03±0.04)	(1.01±0.09±0.06)	(0.45±0.03±0.04)
TPC† [46]			0.65±0.04±0.05	0.50±0.04
29			(0.65±0.04±0.05)	(0.61±0.05±0.06)
ℓN				
μp: EMC [20]	0.84±0.03	1.08±0.10	0.46±0.03	0.73±0.06
$23, 4 < W < 20$				
μN: E665 [22]			0.39±0.02	0.35±0.02
$30, 8 < W < 32$				
νN: BBCNC [21]	0.80±0.04	0.61±0.04	0.64±0.04	0.46±0.03
$> 10, 2.5 < W < 40$				
ep: H1	$0.68 \pm 0.04^{+0.02}_{-0.05}$	$0.52 \pm 0.03^{+0.19}_{-0.21}$	$0.54 \pm 0.03^{+0.03}_{-0.02}$	0.32±0.02±0.06
$300, W \geq 66$				

Table 10: Gaussian fit results for e^+e^- collider experiments with $\sqrt{s} \geq 29$ GeV, and from ℓN scattering experiments at high energies. Where two errors are given the first one is statistical, the second systematical. All entries refer to fits to the double ratios $RR(T)$ without Coulomb and final state corrections. Where available, corrected results are given in brackets. † Values derived from the single ratios $R(T)$.

latter observation confirms, in a new energy regime, earlier work on the search for scale-invariance in multi-hadron production.

Though the evidence for a particle density dependence of the source size, when taken from our data alone is marginal, it seems consistent with the trend observed in hadron-hadron collisions.

Acknowledgements: We are grateful to the HERA machine group whose outstanding efforts made this experiment possible. We appreciate the immense effort of the engineers and technicians who contributed to the construction and the maintainance of the detector. We thank the funding agencies for financial support. We acknowledge the support of the DESY technical staff. We also wish to thank the DESY directorate for the hospitality extended to the non-DESY members of the collaboration.

References

[1] R. Hanbury-Brown, and R. Q. Twiss, Phil. Mag. **45** (1954) 663; idem Nature **178** (1956) 1046; **178** (1956) 1447.

[2] G. Goldhaber et al. , Phys. Rev. Lett. **3** (1959) 181; G. Goldhaber, S. Goldhaber, W. Lee, and A. Pais, Phys. Rev. **120** (1960) 300.

[3] G. Goldhaber, Proc. Workshop on Local Equilibrium in Strong Interaction Physics (LESIP 1), Bad Honnef, Germany (1984), eds. D. K. Scott and R. M. Weiner (World Scientific, Singapore, 1985), p. 115.

[4] W. A. Zajc, in *Hadronic Multiparticle Production*, Advanced Series on Directions in High-Energy Physics, ed. P. Carruthers (World Scientific, Singapore, 1988), vol. 2, p. 235; Proc. Int. Workshop on Correlations and Multiparticle Production (LESIP 4), Marburg, Germany (1990), eds. M. Plümer et al. (World Scientific, Singapore, 1991), p. 439; idem Nucl. Phys. **A525** (1991) 315c.

[5] B. Lörstad, Int. J. Mod. Phys. **A4** (1989) 2861; D. Boal et al., Rev. Mod. Phys. **62** (1990) 553; J. Quebert, Ann. Phys. Fr. **17** (1992) 99; S. Haywood, Rutherford Appleton Laboratory RAL REP. 94-074, 1994.

[6] E. A. De Wolf, Proc. XXVII. Int. Conf. on High-Energy Physics, Glasgow, UK (1994), eds. P. J. Bussey, and I. G. Knowles (IOP-Publishing, Bristol, 1995), p. 1281; S. Pratt in *Quark-Gluon Plasma* **2**, ed. R. C. Hwa (World Scientific, Singapore, 1996), p. 700.

[7] E. A. De Wolf, Proc. XXIV. Symposium on Multiparticle Dynamics, Vietri sul Mare, Italy (1994), eds. A. Giovannini et al. (World Scientific, Singapore 1995), p. 15.

[8] E. A. De Wolf, L. M. Dremin, and W. Kittel, Phys. Rep. **270** (1996) 1.

[9] J. D. Bjorken, Proc. XXIV. Symposium on Multiparticle Dynamics, Vietri sul Mare, Italy (1994), eds. A. Giovannini et al. (World Scientific, Singapore, 1995), p. 611.

[10] K. Kolehmainen, and M. Gyulassy, Phys. Lett. **B180** (1986) 203.

[11] M. G. Bowler, Particle World **2** (1991) 1.

[12] J. D. Bjorken, Phys. Rev. **D27** (1983) 140.

[13] X. Artru, and G. Menessier, Nucl. Phys. **B70** (1974) 93.

[14] B. Andersson, and W. Hofmann, Phys. Lett. **B169** (1986) 364.

[15] M. G. Bowler, Z. Phys. **C29** (1985) 617; X. Artru, and M. G. Bowler, Z. Phys. **C37** (1988) 293.

[16] A. Bialas, Nucl. Phys. **A545** (1992) 285c; idem Acta Phys. Pol. **B23** (1992) 561.

[17] P. Abreu et al., DELPHI-Coll., Z. Phys. **C63** (1994) 17.

[18] I. V. Ajinenko et al., EHS/NA22-Coll., Z. Phys. **C61** (1994) 567.

[19] N. Neumeister et al., UA1-Coll., Z. Phys. **C60** (1993) 633.

[20] M. Arneodo et al., EMC-Coll., Z. Phys. **C32** (1986) 1.

[21] V. A. Korotkov et al., BBCNC Coll., Z. Phys. **C60** (1993) 37.

[22] M. R. Adams et al., E665-Coll., Phys. Lett. **B308** (1993) 418.

[23] S. Aid et al., H1-Coll., Nucl. Phys. **B470** (1996) 3.

[24] T. Ahmed et al., H1-Coll., Phys. Lett. **B348** (1995) 681; idem Nucl. Phys. **B429** (1994) 477; S. Aid et al., H1-Coll., Z. Phys. **C70** (1996) 609.

[25] M. Derrick et al., ZEUS-Coll., Phys. Lett. **B315** (1993) 481; ibid. **B332** (1994) 228; ibid. **B338** (1994) 483; idem Z. Phys. **C70** (1996) 391.

[26] I. Abt et al., H1-Coll., Nucl. Instr. Meth. **A386** (1997) 310; ibid. 348.

[27] S. Aid et al., H1-Coll., Nucl. Phys. **B480** (1996) 3.

[28] S. Aid et al., H1-Coll., Nucl. Phys. **B472** (1996) 3.

[29] A. Blondel, and F. Jacquet, Proc. of the Study of an ep Facility for Europe, ed. U. Amaldi (DESY, Hamburg, 1979), DESY-Report 79-48 (1979) 391.

[30] C. Dollfus, Ph.D. Thesis, University of Zürich (1996), unpublished.

[31] E. Rizvi, Ph.D. Thesis, Queen Mary and Westfield College, London (1997), unpublished.

[32] T. Eckel, Diploma Thesis, University of Hamburg, H1-report H1-08/94-371 (DESY, 1994), unpublished.

[33] G. Ingelman, Proc. HERA workshop, eds. W. Buchmüller, and G. Ingelman (DESY, Hamburg, 1991), vol. 3, p. 1366.; LEPTO 6.1 TSL/ISV-92-0065.

[34] G. Ingelman et al., LEPTO 6.4 unpublished manual.

[35] G. Gustafson, and U. Petterson, Nucl. Phys. **B306** (1988) 746; G. Gustafson, Phys. Lett. **B175** (1986) 453; B. Andersson et al., Z. Phys. **C43** (1989) 625.

[36] L. Lönnblad, Comp. Phys. Comm. **71** (1992) 15.; ARIADNE 4.03 unpublished manual.

[37] M. Bengtsson, and T. Sjöstrand, Z. Phys. **C37** (1988) 465.

[38] G. A. Schuler, and H. Spiesberger, Proc. HERA workshop, eds. W. Buchmüller, and G. Ingelman (DESY, Hamburg, 1991), vol. 3, p. 1419.; DJANGO 6.0 unpublished manual.

[39] A. Kwiatkowski, H. Spiesberger, and H.-J. Möhring, Proc. HERA workshop, eds. W. Buchmüller, and G. Ingelman (DESY, Hamburg, 1991), vol. 3, p. 1294; A. Kwiatkowski, H. Spiesberger, and H.-J. Möhring, Comput. Phys. Comm. **69** (1992) 155.

[40] H. Jung, Comp. Phys. Comm. **86** (1995) 147.

[41] H1-Coll., Contr. paper to Int. Conf. High-Energy Phys. ICHEP'96, Warsaw (Poland) PA-02-061.

[42] T. Sjöstrand, Comput. Phys. Comm. **82** (1994) 74.

[43] L. Lönnblad, and T. Sjöstrand, Phys. Lett. **B351** (1989) 293.

[44] R. Brun et al., GEANT3, CERN DD/EE/84-1 (1987).

[45] D. Decamp et al., ALEPH-Coll., Z. Phys. **C54** (1992) 75.

[46] H. Aihara et al., TPC-Coll., Phys. Rev. **D31** (1985) 996.

[47] S. K. Choi et al., AMY-Coll., Phys. Lett. **B355** (1995) 406.

[48] P. Avery et al., CLEO-Coll., Phys. Rev. **D33** (1985) 2294.

[49] A. E. Blinov et al., VEPP-Coll., Z. Phys. **C69** (1996) 215.

[50] M. G. Bowler, Phys. Lett. **B270** (1991) 69.

[51] M. Biyajima et al., Phys. Lett. **B353** (1995) 340.

[52] M. Suzuki, Phys. Rev. **D35** (1987) 3359.

[53] N. M. Agabyan et al., EHS/NA22-Coll., Z. Phys. **C46** (1990) 387.

[54] N. Neumeister et al., UA1-Coll., Phys. Lett. **B275** (1992) 186.

[55] P. Abreu et al., DELPHI-Coll., Phys. Lett. **B286** (1992) 201.

[56] P. D. Acton et al., OPAL-Coll., Phys. Lett. **B267** (1991) 143.

[57] M. G. Bowler, Z. Phys. **C39** (1988) 81.

[58] S. Aid et al., H1-Coll., Z. Phys **C72** (1996) 573.

[59] G. Alexander et al., OPAL-Coll., Z. Phys. **C72** (1996), 386.

[60] E. L. Berger et al., Phys. Rev. **D15** (1977) 206.

[61] M. Althoff et al., TASSO-Coll. Z. Phys. **C30** (1986) 355.

[62] I. Juričič et al., MARK II-Coll., Phys. Rev. **D39** (1989) 1.

[63] T. Åkesson et al., AFS-Coll., Phys. Lett. **B129** (1983) 269; ibid. **B187** (1986) 420; A. Breakstone et al., SFM-Coll., Z. Phys. **C33** (1987) 333.

[64] C. Albajar et al., UA1-Coll., Phys. Lett. **B226** (1989) 410.

[65] T. Alexopoulos et al., E735-Coll., Phys. Rev. **D48** (1993) 1931.

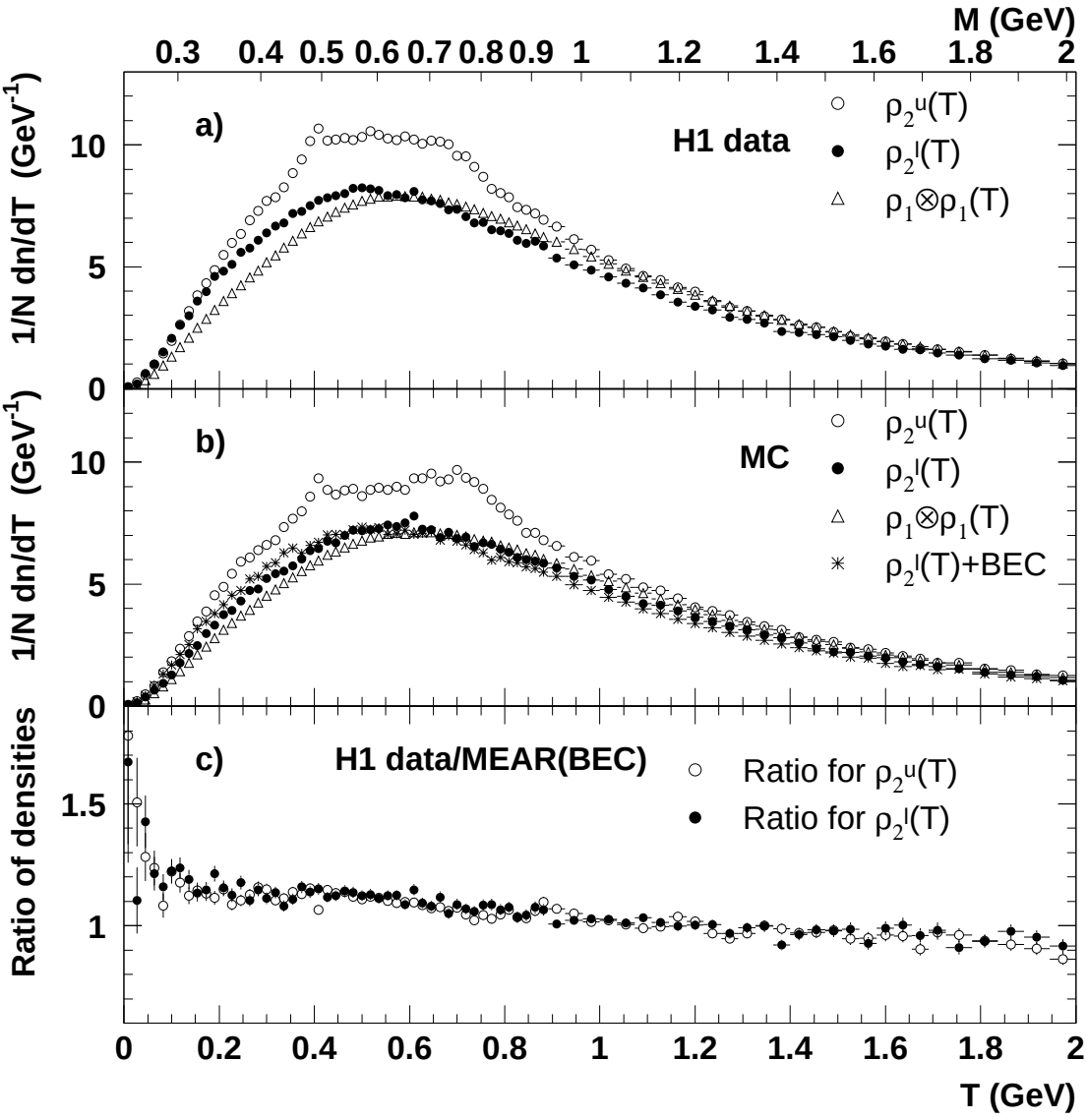

Figure 1: Non-diffractive events - **a)** Inclusive two-particle densities as a function of T for data: full circles denote the like-sign pairs, $\rho_2^l(T)$; open circles unlike-sign pairs, $\rho_2^u(T)$; open triangles the density obtained from mixing events, $\rho_1 \otimes \rho_1(T)$. **b)** Inclusive two-particle densities for reconstructed MEAR Monte Carlo events as in (a). MEAR(BEC) predictions for like-sign pairs are indicated as stars. **c)** Ratios of data to reconstructed MEAR(BEC) for the like and unlike-sign densities.

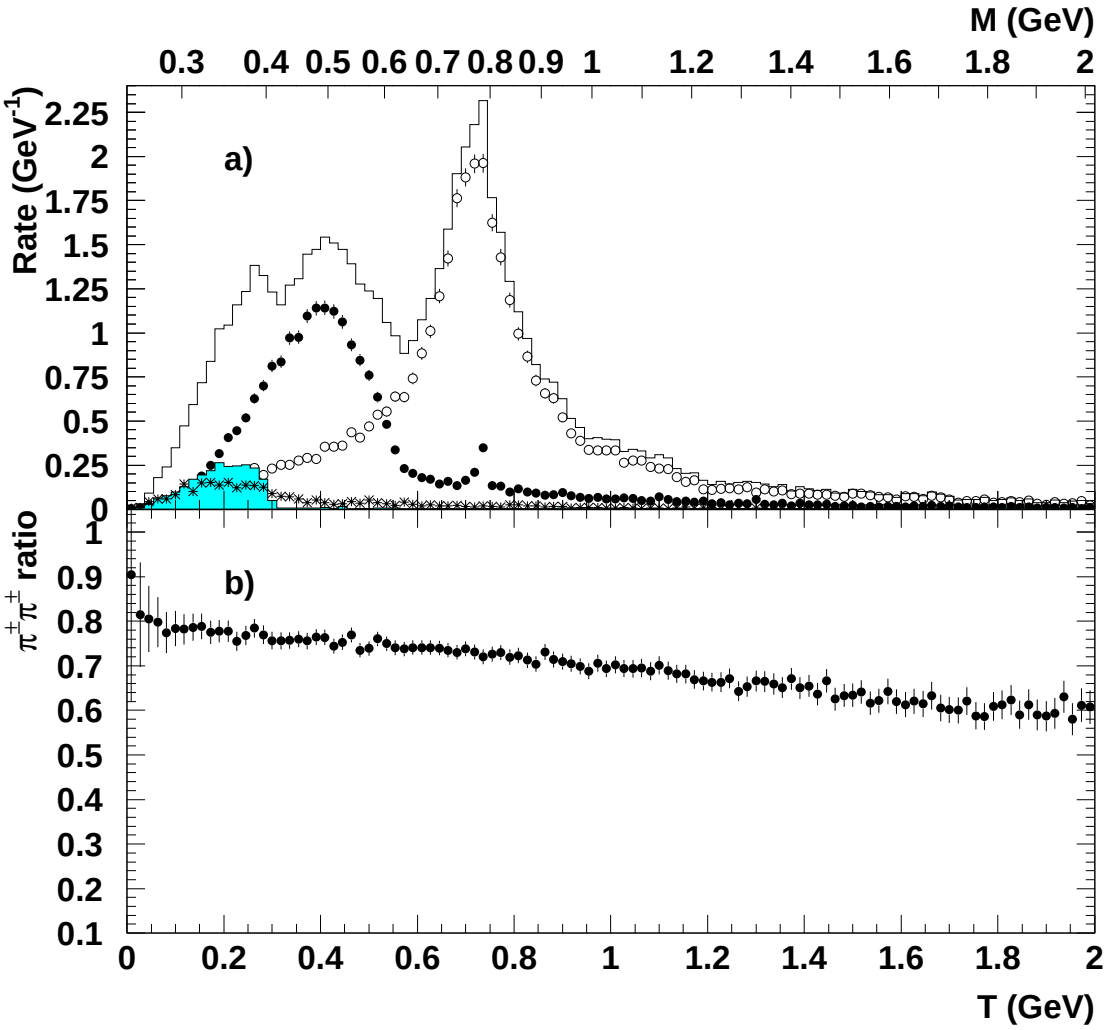

Figure 2: **a)** MEAR Monte Carlo predictions for the invariant mass distributions for unlike-sign pion pairs from the decays of the following particles: ω (full circles), ρ (open circles) and η (shaded-histogram). The full histogram is the sum of all three contributions. The contribution to the like-sign density from η' decays is shown as stars. **b)** MEAR Monte Carlo prediction for the ratio of densities for $\pi^{\pm}\pi^{\pm}$ pairs to that of all like-sign charged tracks pairs.

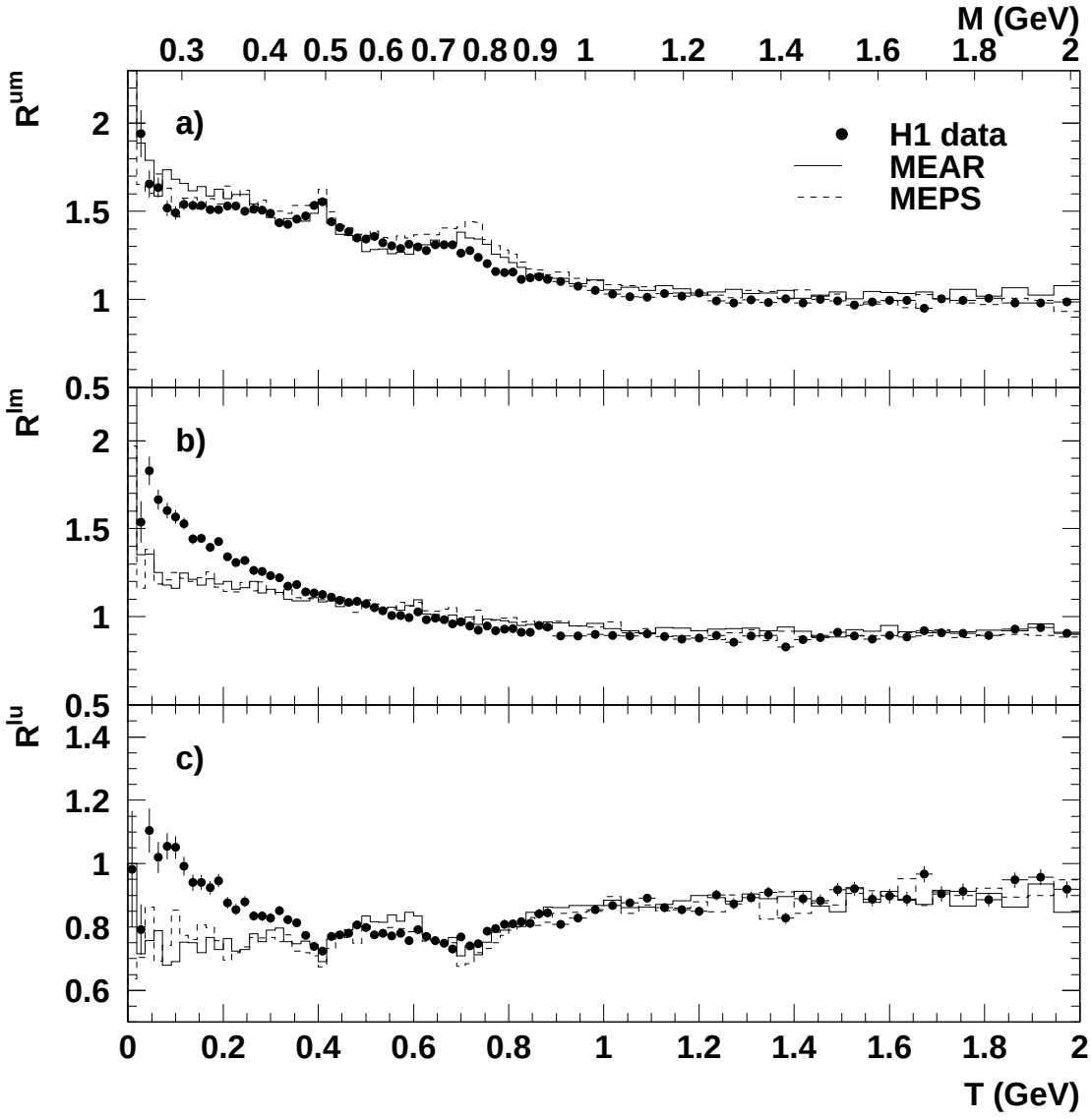

Figure 3: Comparison of the non-diffractive data (filled circles) with the MEAR (solid line) and MEPS (dashed line) Monte Carlo simulations for the ratios: **a)** $R^{um}(T)$, **b)** $R^{lm}(T)$ and **c)** $R^{lu}(T)$.

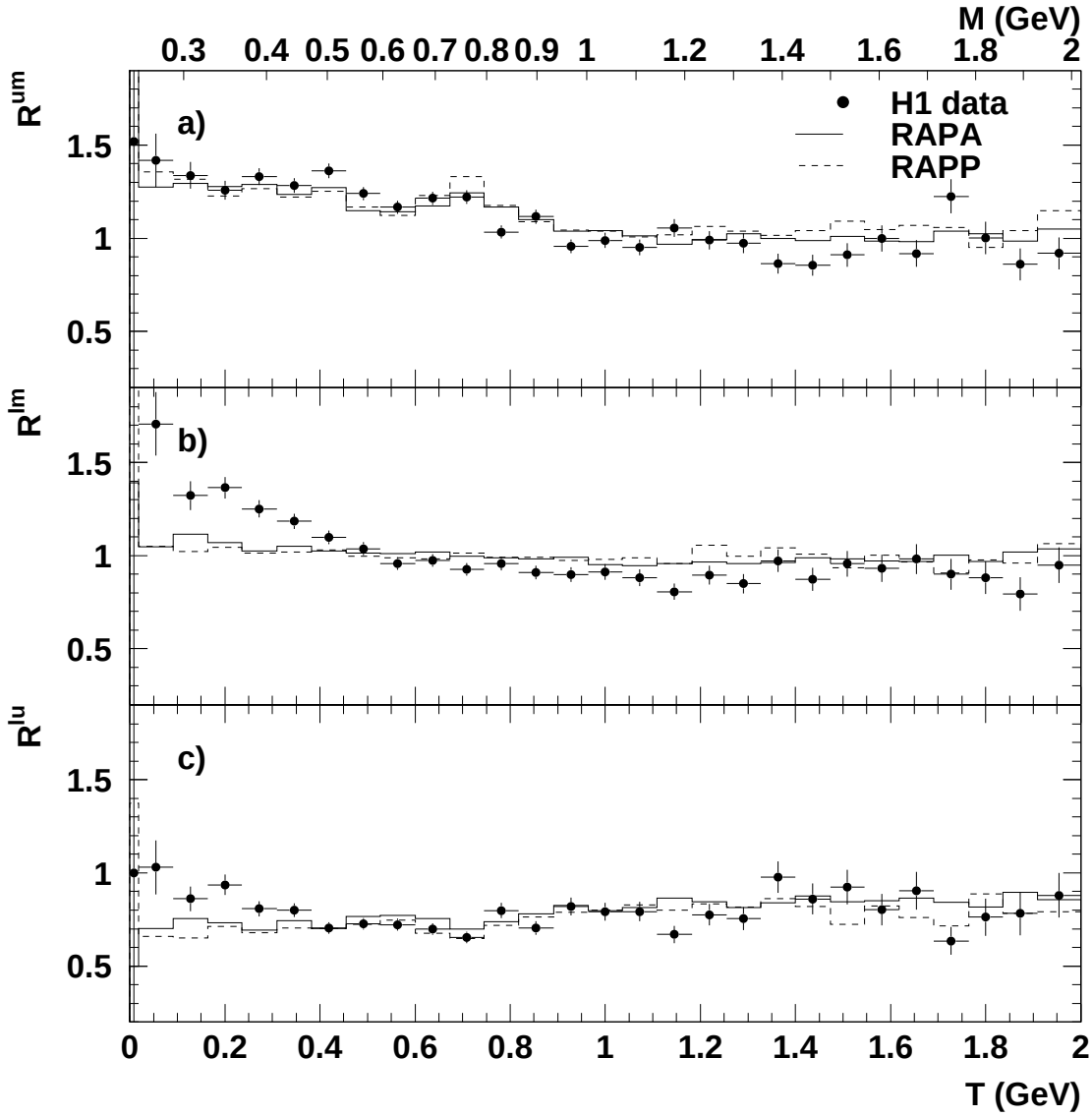

Figure 4: Comparison of the diffractive data (filled circles) with the RAPA (solid line) and RAPP (dashed line) Monte Carlo simulations for the ratios: **a)** $R^{um}(T)$, **b)** $R^{lm}(T)$ and **c)** $R^{lu}(T)$.

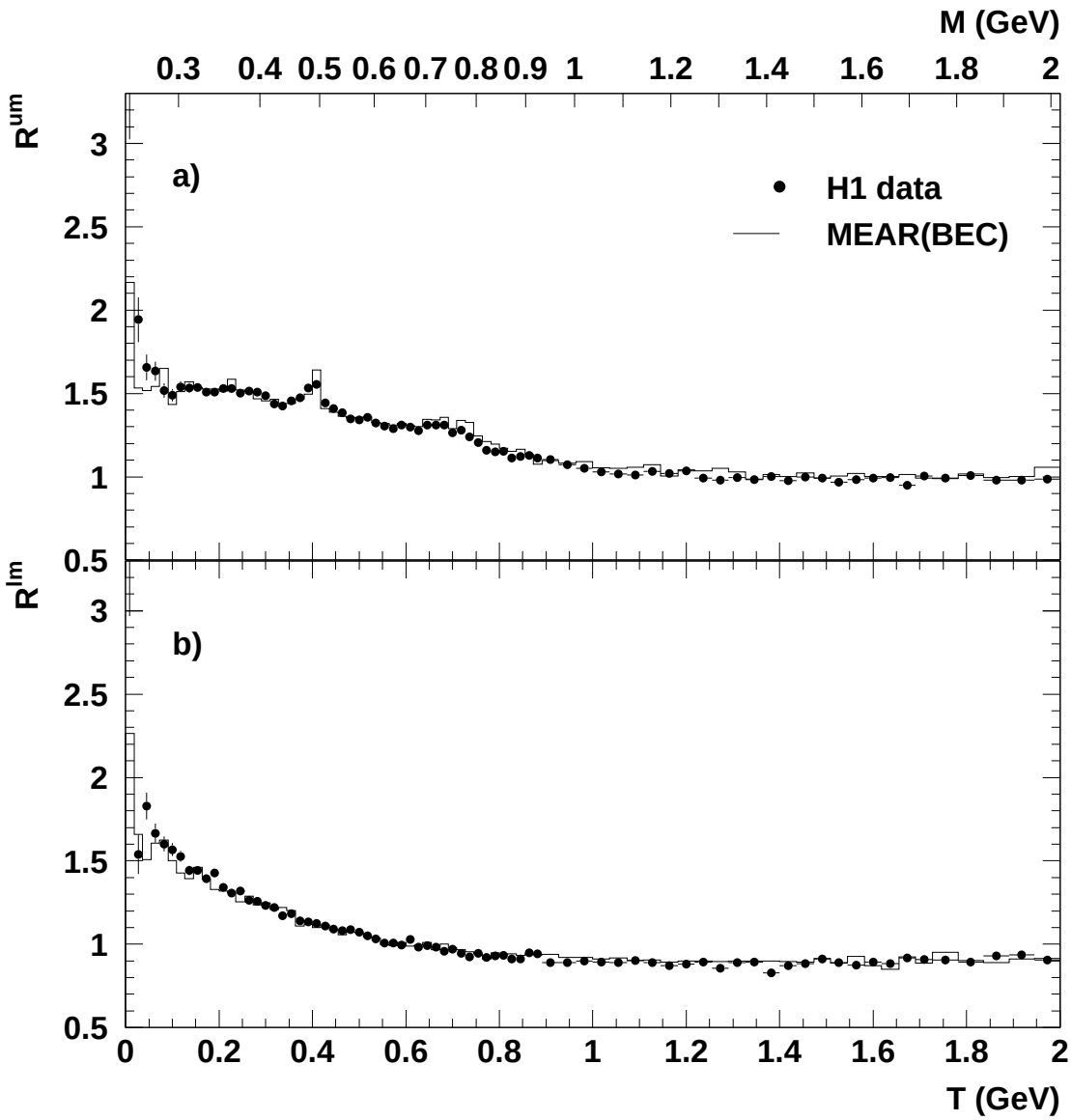

Figure 5: Comparison of the non-diffractive data (filled circles) with the MEAR(BEC) simulation for the ratios: **a)** $R^{um}(T)$ and **b)** $R^{lm}(T)$.

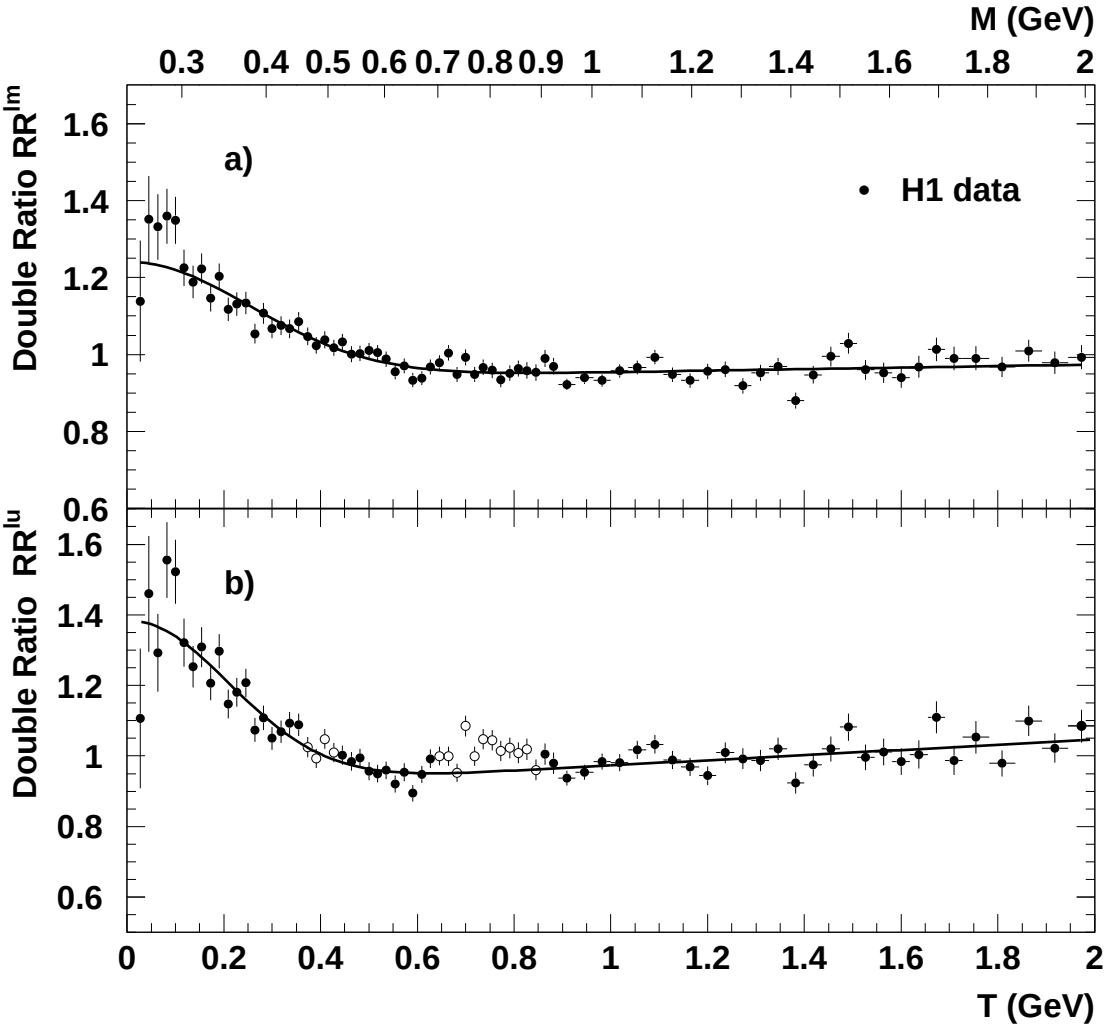

Figure 6: **a)** The non-diffractive data for the double ratio RR^{lm}. **b)** The non-diffractive data for the double ratio RR^{lu}. The data points marked by open circles have not been included in the fit. The solid curve results from a fit to the Gaussian parametrisation of Eq. (14).

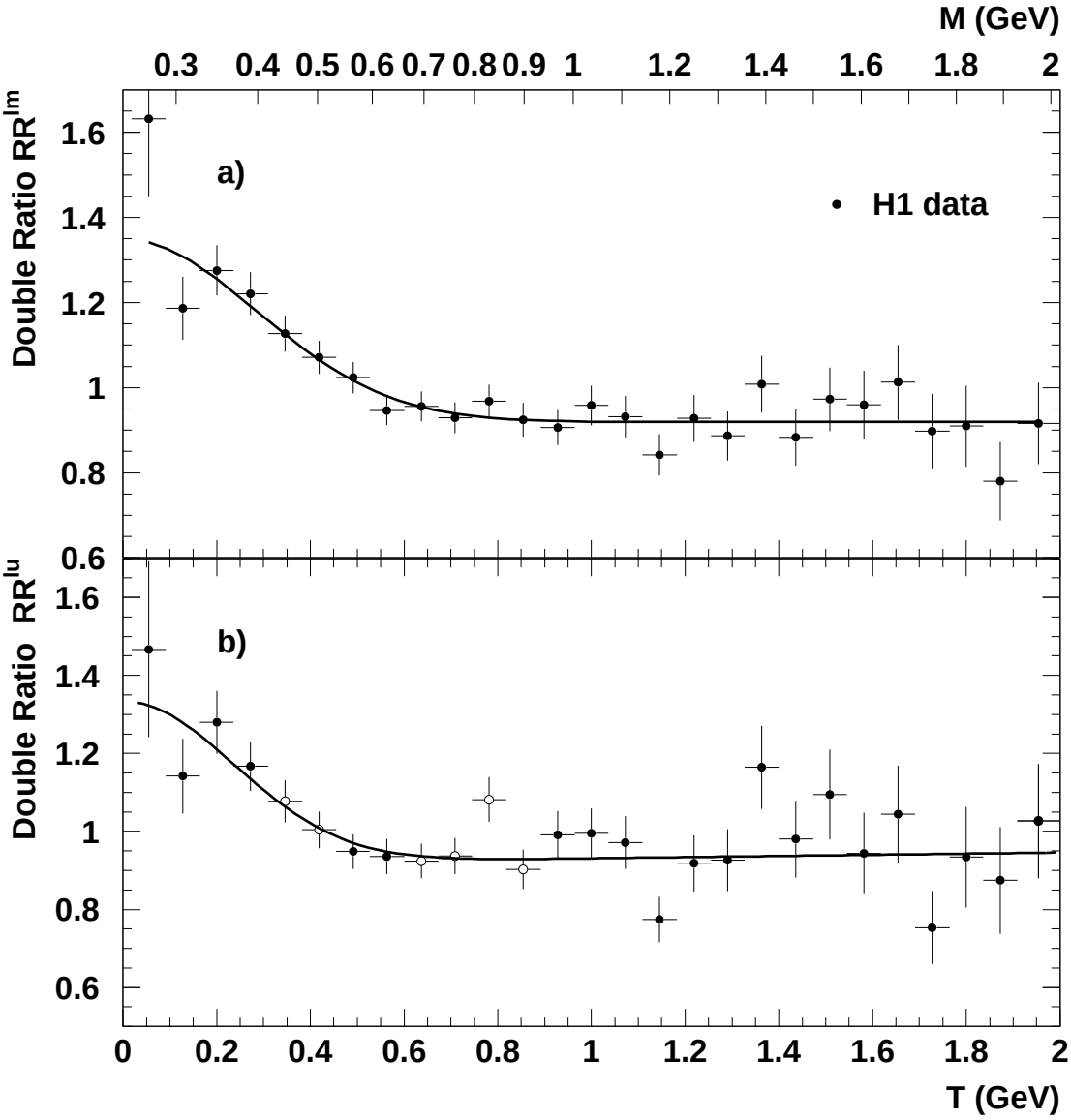

Figure 7: The diffractive data for the double ratio RR^{lm} **(a)** and RR^{lu} **(b)**. The data points marked by open circles have not been included in the fit. The solid curve results from a fit to the Gaussian parametrisation of Eq. (14).

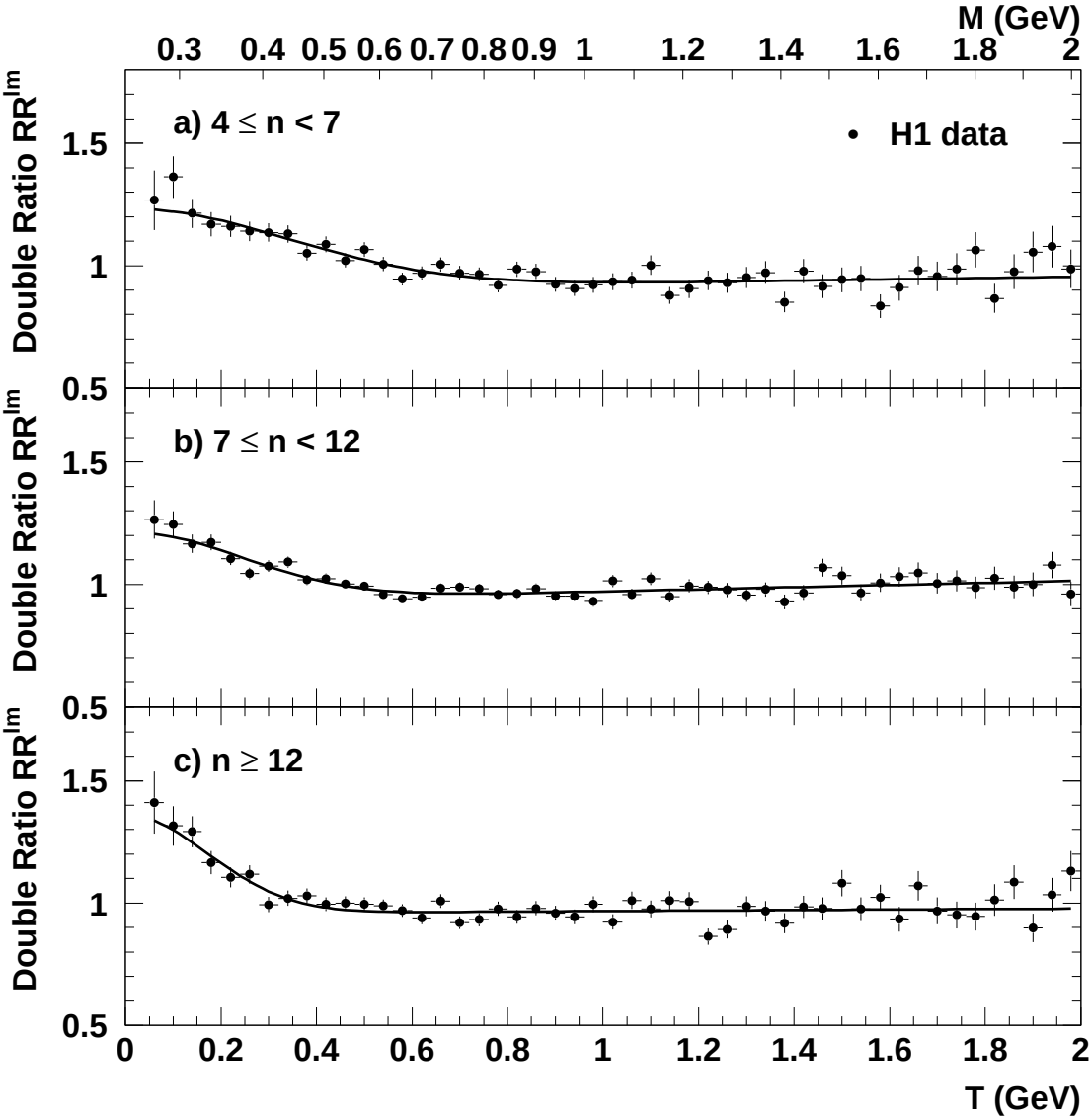

Figure 8: The double ratio RR^{lm} for the non-diffractive data sample in intervals of *observed* multiplicity. The curves are fits to the Gaussian parametrisation of Eq. (14).

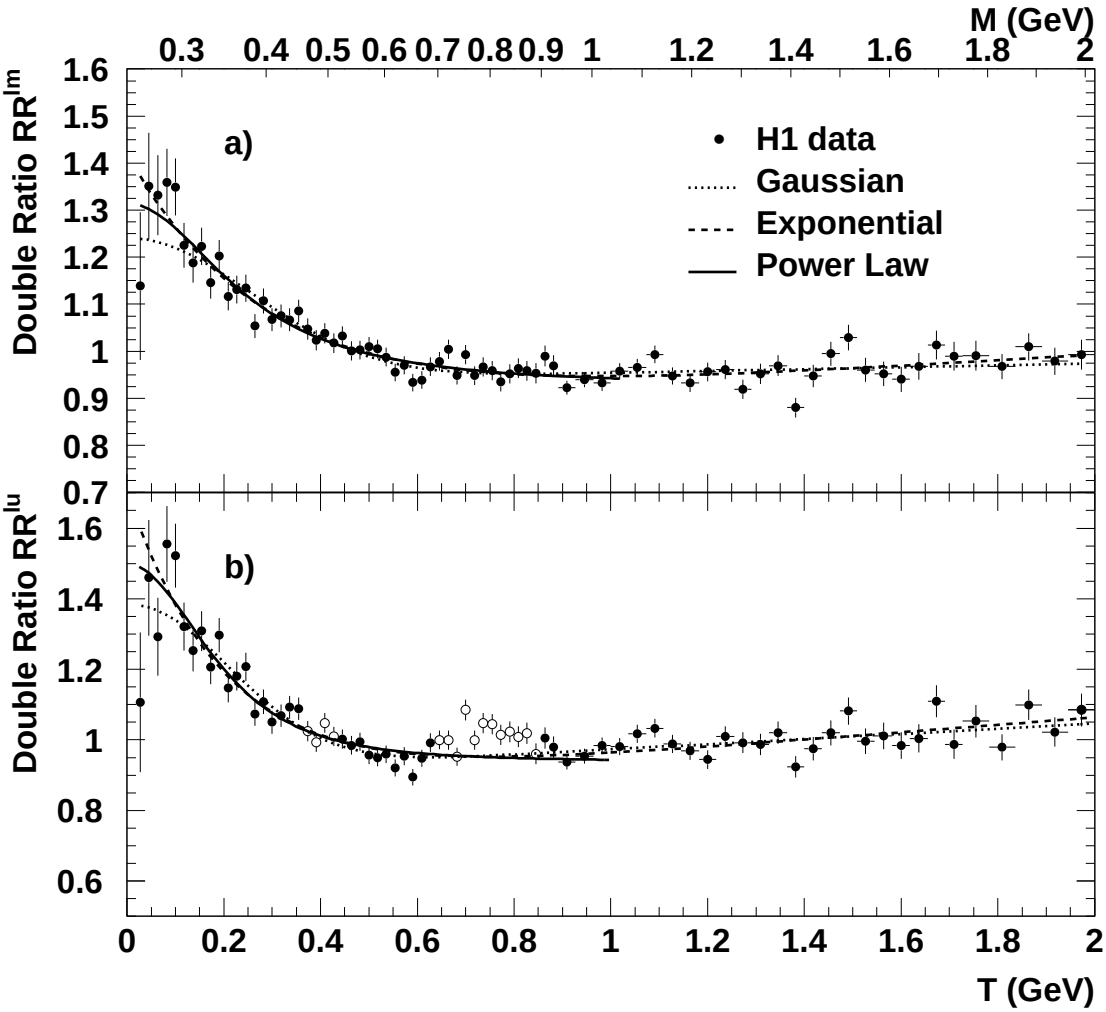

Figure 9: The double ratios **a)** $RR^{lm}(T)$, **b)** $RR^{lu}(T)$ for the non-diffractive data fitted to the Gaussian (Eq. (14)), exponential (Eq. (15)) and power law (Eq. (7)) parametrisation.

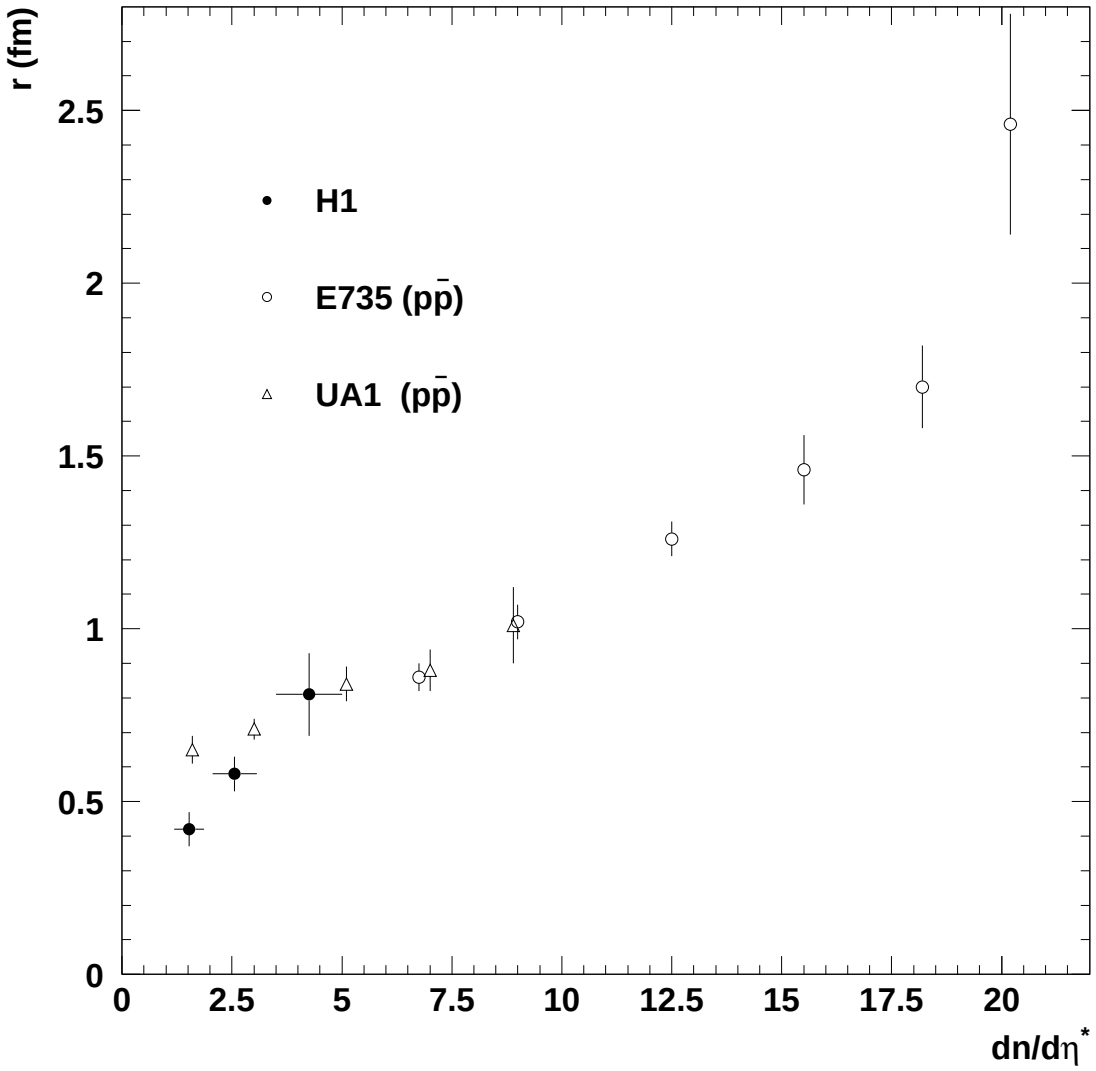

Figure 10: The radius parameter r versus charged particle density. The full circles are from this analysis, the open circles (triangles) are from $p\bar{p}$ collisions at a centre of mass energy of 1.8 TeV [65] and 630 GeV [64]. Only statistical errors are shown.